Book chapter in "Soft Matter: Scattering, Imaging and Manipulation", Vol. 4
edited by R. Borsali and R. Pecora, Springer (2007)(in press)

Chapter #

Single-Molecule Studies of DNA

Visualization and Manipulation of Individual DNA Molecules with Fluorescence Microscopy and Optical Tweezers

John Peter Rickgauer and Douglas E. Smith*

Department of Physics, University of California, San Diego, USA.
*To whom correspondence should be addressed. e-mail: des@physics.ucsd.edu

1. INTRODUCTION

Scientific interest in visualizing and characterizing the dynamics of individual biomolecules has increased considerably over the last fifteen years, a fact that has been reflected in the impressive development of techniques designed to work with precision at the sub-micron level. Two of the most insightful techniques that have been developed in this pursuit are fluorescence microscopy and optical tweezers: the former permits a passive visualization of the position, conformation, and dynamics of single molecules, and the latter allows interactive mechanical manipulation of the forces acting on single molecules. Taken together, the two complementary methods have enabled a spectrum of measurements that have given visual -- and even tactile! -- character to the single-molecule regime.

While methods preceding single-molecule biophysics did offer insights into molecular dynamics, these characterizations were derived mainly from "bulk" methods. These methods measure average behavior of ensembles of molecules, and necessarily ignored properties such as uncorrelated fluctuations in the dynamics of single molecules. Simultaneously, theorists approached the challenge of single-molecule characterization from the opposite side, proposing models of single molecule behavior in order to predict the properties measured by ensemble studies. Now, with the development of single-molecule biophysics, these ensemble studies and single-molecule theories are being extended through a set of techniques that examine the properties of individual molecules in real time, and present the opportunity to test previously inscrutable theories of single-molecule behavior.

In this chapter we will discuss these two single-molecule techniques *per se*, as well as some of their applications that have been helpful in understanding the physical properties of DNA and protein-DNA interactions.

2. FLUORESCENCE IMAGING

In this section we will discuss fluorescence imaging methods and their application to studies of single-DNA dynamics in dilute and entangled solutions subject to flow, in two-dimensional confined geometries, and in electrophoresis. Then we will briefly discuss studies of protein-DNA binding and the use of single-pair fluorescence energy resonance transfer (FRET) to study molecular conformation.

2.1 Polymer Physics and Rheology

Polymer physics and rheology are concerned with understanding non-Newtonian flow properties exhibited by polymeric fluids [1]. Whereas simple Newtonian fluids exhibit intuitive, viscous behavior, polymeric fluids exhibit surprising "viscoelastic" behavior. In example, consider what happens when you stir your cup of coffee, and then stop: the coffee continues to swirl in the direction your spoon was rotating, and eventually comes to a stop through viscous dissipation. On the other hand, if your coffee were comprised of long, flexible polymers, it would -- besides being a pretty unconvincing cup of coffee -- exhibit a striking rotational recoil after the forward rotation had stopped, spinning in the direction *opposite* to your stir. This counter-rotation occurs because the polymers within the fluid become stretched during the initial rotational flow flow, recoiling once it stops. An early example of the beneficial interface between biology and physics This physical, polymeric understanding of molecular behavior was applied in the days preceding modern sequencing techniques by Zimm and colleagues, who cleverly used a bulk polymer assay to estimate the length of individual bacterial genome sizes [2].

Polymeric fluids also have flow-dependent viscosities, and exhibit normal stress (where a fluid sheared between two parallel plates exerts force in the perpendicular direction). Besides being of practical importance in the chemical and petroleum industries polymer fluid properties are of fundamental interest to soft matter physicists. Molecular biologists also stand to gain a great deal from a better characterization of biopolymers such as DNA, as many important biological techniques depend critically upon controlled polymer physics. Gel electrophoresis, for example, of singular importance in molecular biology for estimating the size of genetic sequences, and future improvements in the efficiency and efficacy of the technique rely almost uniquely upon understanding the dynamics of individual strands of DNA as they move through a fluid solution.

Despite the many practical applications that bulk studies of polymers have yielded a complete theoretical explanation of the molecular dynamics underlying rheology and electrophoresis has not been developed. Thus, an important goal of current polymer physics is to establish a connection between the microscopic and macroscopic properties of polymeric solutions. In many cases, single-molecule imaging of polymer dynamics can be used to test existing theoretical models. For many decades polymer dynamics was experimentally studied by indirect methods such as bulk rheology, light-scattering, and birefringence. Theoretical polymer dynamics, on the other hand, focused mostly on describing single-polymer dynamics to improve models of bulk properties, and although the accompanying bulk-assay experiments were able to test these theories' predictive

accuracy, they were often unhelpful in testing the molecular assumptions underlying the predictions. Direct fluorescence imaging of single polymer dynamics, however, has allowed both the assumptions and the predictions of these theories to be tested.

2.2 Basic Single DNA Imaging Methods

Although the contour length of DNA is commonly at least several μm, the molecule's axial diameter is only ~2 nm, making it impossible to visually resolve single molecules with ordinary bright-field microscopy. By binding fluorescent dye molecules along the length of the DNA and exciting these dyes with specific wavelengths of light, one can beat this limitation, recording the emissive response of the molecules -- which emit at a longer wavelength than that of the excitation wavelength -- and thus visually resolving characteristics of the subject DNA.

Fluorescent labeling: YOYO (oxazole yellow dimer) is the dye most often used for single-DNA imaging, and is among the highest sensitivity fluorescent probes currently available [3]. It is effectively non-fluorescent in solution, exhibiting a 100- to 1000-fold fluorescence enhancement upon binding to DNA, which helps distinguish labeled molecules from visual background noise. When bound to DNA, YOYO can be stimulated by blue light, and will respond with emission in green. While many other nucleic acid-specific dyes exist, such as DAPI and ethidium bromide, YOYO's high brightness and relative photostability make it generally advisable for single-DNA imaging.

Epifluorescence microscopy: The setup of a basic epifluorescence microscope is shown schematically in Fig. 1. Samples are illuminated and imaged through a single microscope objective lens, with the excitation light traveling in the opposite direction as the collected fluorescence light. This design minimizes the amount of backscattered excitation light, which in turn increases the contrast between the molecule and the background. Other fluorescence microscopy configurations, such as confocal and total internal reflection fluorescence imaging, are desirable for certain specific types of experiments, and shall be discussed in examples below. In general, the success of a fluorescence setup depends upon the ability to discriminate between the excitation light and emitted fluorescence.

Optical Resolution: The ability to observe the finer details of DNA conformation is limited by the optical resolution of the experimental microscope, a feature determined primarily by the numerical aperture (NA) of the objective lens. Relevant NAs range between 1.4 for oil-immersion and 1.2 for water-immersion objectives, where each "immersion" type is designed to interface with a fluid (oil or water, respectively) between the objective and the sample coverglass to improve light-collection from samples. Despite its slightly smaller NA, a water-immersion objective is generally better suited for focusing deep into aqueous samples, as the water interface corrects for related spherical aberrations, and thus improves the quality of the image.

The theoretical limit of a fluorescence setup's optical resolution may be found by $R=0.61\lambda/NA$ [4]. An objective with an NA of 1.2, for example, is limited by this

relationship to resolving objects separated by distances larger than ~300 nm. A resolution of 300 nm does not allow *exact* imaging of DNA conformation, since DNA typically bends on a length scale smaller than 50 nm; the best images of relaxed, coiled DNA molecules, then, still appear in successful fluorescence imaging as bright "blobs." Fortunately, more detailed observations become possible when molecules longer than a few microns are elongated by a flow, for instance, or by gel electrophoresis.

It's also important to note that resolution limits only dictate the smallest resolvable distance between two *points*, and that the location of the centroid of an isolated fluorescent molecule can be determined with a precision approaching ~1 nm with proper image processing. In this way single-molecule diffusion and transport can be tracked with high sensitivity [5,6].

Photobleaching: One challenge inherent to fluorescence imaging is the tendency of images to fade, a consequence of photo-induced chemical damage to the dye molecules. YOYO-labeled DNA, for instance, can meet with "photobleaching": if dissolved oxygen (a catalyst of photobleaching) is not removed from the subject solution, fluorescent images can fade in seconds. Worse still, the same chemical changes that cause photobleaching can break up DNA into small, meaningless fragments. Addition of β-mercaptoethanol (a reducing agent) and a glucose, glucose oxidase, and catalase (which act to remove dissolved oxygen) are effective counters to photobleaching . Under optimal chemical conditions and minimal excitation intensity, single DNA molecules can produce visible fluorescence for up to several hours [7]. In this way, a statistical ensemble of conformations, which may be compared against bulk assays of the same nature, can be compiled by observing a single molecule.

2.3 Single DNA Dynamics: Theory Meets Experiment

Development of Single DNA Imaging Methods: To our knowledge, M. Yanagida and colleagues were the first to image single DNA molecules with fluorescence techniques [8]. They observed that the DNA formed a coiled structure at equilibrium and noted its Brownian motion [9,10]. Later, several groups observed the motion of individual DNA molecules undergoing gel electrophoresis [11,12]. S. Chu and colleagues were the first to demonstrate simultaneous manipulation and visualization of single DNA molecules combining optical tweezers, microfluidics, and fluorescence microscopy [13-16]. Bustamante and colleagues were pioneers as well, employing fluorescence imaging combined with magnetic and hydrodynamic forces (and later optical tweezers) to manipulate and stretch single DNA molecules [17,18].

Relaxation: The relaxation of stretched polymers is of fundamental importance in determining the rheological behavior of polymeric fluids, and can be generally understood as the product of competing entropic elasticity and hydrodynamic drag. These effects were first modeled in detail by Zimm, who treated the chain as a string of hydrodynamically interacting beads connected by springs. Zimm's model predicted that the relaxation of a polymer modeled as such would exhibit modes with time constants scaling as a power of the contour length of the DNA [19].

Perkins *et al*. used fluorescence microscopy to measure such relaxation of single DNA molecules by stretching them in a flow, marking the length of individual stretched molecules, and then observing them as they relaxed (Fig. 2) [16]. Fitting these relaxation data to a continuous spectrum of decaying exponentials revealed that the DNA molecules of varying lengths possessed distinct internal relaxation modes, wherein characteristic relaxation times were proportionate to time constants dependent upon molecular length (L) (Fig. 3). The longest relaxation time scaled as $L^{1.65}$, in agreement with dynamic scaling predictions of the Zimm model.

Diffusion: An interesting prediction of the Zimm model was that the hydrodynamic screening of the interior of a coiled molecule would affect its diffusional dynamics. In 1992, Matsumoto *et al.* recorded the Brownian motion of free-floating molecules of T4 DNA (166 kbp, or 56 μm, in length) and found that the rotational relaxation, radius of gyration (an RMS measure of coil size), and conformational fluctuations were in reasonable agreement with the Zimm model [20]. Translational diffusion coefficients were determined by tracking Brownian motion and determining the mean-square displacement versus time. The translational diffusion coefficients were lower than the model predicted, a deviation ascribed to the experimentally unpredictable hydrodynamic interactions between subject molecules and the walls of the thin sample chamber. Subsequent measurements by Smith, Perkins, and Chu (Fig. 4) employed deeper sample chambers to eliminate this hydrodynamic interaction, and found that under these conditions, the diffusion coefficient scaled as $L^{-3/5}$, in agreement with the Zimm model [21].

Hydrodynamic Drag: According to the Kirkwood-Riseman theory of hydrodynamic interactions, a long polymer's interior shielding is expected to become negligible when it is highly stretched [19]. Theoretical expectations held that in this limit, the end-to-end extension of a polymer in a uniform flow would be a universal function of the flow velocity multiplied by a polymer's length (vL).

However, measurements by Perkins *et al*. revealed that the extension of DNA (tethered at one end by optical tweezers) scaled as $vL^{0.54}$ for molecules between 22 and 84 μm, suggesting that hydrodynamic interactions were not, in fact, negligible [22]. Further calculations explained this unexpected result as a consequence of the small ratio of DNA's extended- and coiled-state drag coefficients, a relationship produced by its relatively long persistence length (~50nm) and relatively narrow hydrodynamic diameter (~2 nm) [23]. Thus, DNA molecules of these lengths, despite their large aspect ratio, cannot be correctly simplified by applying the long-length limit of polymer hydrodynamic theory. Further studies on longer chains of up to ~150 μm in length revealed an increase in the apparent scaling exponent to 0.76, indicating that this parameter only slowly approaches the expected limit as the chain length is increased.

Normal Mode Fluctuations: When a polymer is partially stretched and anchored at both ends, it will undergo fluctuations in the amplitudes of its normal oscillatory modes due to Brownian motion. The feasibility of describing such fluctuations using a strict normal mode representation of superimposed orthogonal states had been questioned, however,

since it was thought that the nonlinear hydrodynamic interactions of polymer chains could render this linear model incomplete [24].

In 1997, Quake, Babcock, and Chu stretched single DNA molecules between two beads held by optical tweezers, creating partial extensions that would undergo normal-mode oscillations, and digitized fluorescently produced images of the chain contour [25]. They showed that, contrary to concerns about complex nonlinear components, the oscillatory dynamics of partially stretched lambda-phage DNA molecules could be described aptly by a linear orthogonal normal mode superposition: the relaxation times of variously extended molecules were plotted against mode numbers, and the results were fit by a power law with an exponent of ~1.7. This fit of power laws to the observed oscillations suggested that stretched DNA exhibited a traditional linear behavior in its normal-mode oscillations, and thus that the nonlinear contributions of the polymer's hydrodynamic interactions were, in fact, negligible.

2.4 Single DNA Dynamics in Fluid Flow

The field of rheology is concerned with the behavior of macromolecular fluids under the influence of flow. Our focus here is on single-molecule rheology, which attempts to understand the behavior of individual polymers under controlled fluidic flows.

Following the introduction of experimentally viable fluorescence imaging, initial measurements in fluid flow were conducted mostly with dilute polymers in two-dimensional flows, a fact that reflects the convenience of two-dimensional imaging. There are two fundamental types of flow fields, extensional and rotational, which linearly superpose to produce further, more-complex flows in two dimensions.

Extensional flow is characterized by a velocity gradient along the direction of the flow, and this gradient may be modulated to stretch polymers to varying fractional extensions of their total contour length. Rotational flow is comprised of a circulating vector field through which polymers tumble and rotate. Shear flow describes an equal mixture of extensional and rotational flow, and possesses a velocity gradient in a direction perpendicular to the flow. Any unbalanced combination of the two fundamental types of flow creates a "mixed flow."

Extensional Flow: The potential of an extensional flow to deform a polymer can be described by the Deborah number (*De*), defined as the strain rate (the applied velocity gradient) multiplied by the time polymer relaxation time (the time required for a deformed polymer to resume its natural, unperturbed conformation). In 1974, de Gennes predicted that polymers would display an abrupt coil-stretch transition at a critical *De* of order one, and moreover, that hysteresis might be observed near this transition [26].

In 1997, Perkins, Smith, and Chu combined controlled rheological techniques with fluorescence imaging in order to investigate de Gennes' claim [27,28]. The group designed a microfluidic cell with two crossed orthogonal channels to produce a pure extensional flow in which slow-moving molecules could be extended in the vicinity of a stagnation point (Fig. 5). They found that, in reasonable agreement with theory, all molecules tended toward a final state of complete extension for cases of $De>0.4$. In these lambda-phage DNA experiments, no definite hysteresis was observed, though Schroeder

et al. later reported hysteresis when a similar set of measurements were carried out with 1600 μm-long *E. Coli* DNA [29].

Intriguingly, the stretching dynamics were highly heterogeneous. Individual molecules exhibited transient conformations with vastly differing dynamics, prompting de Gennes to coin the term “molecular individualism" to describe this behavior. Rather than following the expected, statistically average path of elongation over time, single molecules displayed a wide variety of stretching rates. Within conformationally distinguishable groups, general trends were observable, and individual molecules within them again displayed heterogeneous dynamics. Chains that developed a “dumbbell” shape, for example, stretched faster on average than ones that developed a “folded” shape, and within each grouping, a continuum of transient conformations were observed. Experiments and simulations revealed that these heterogeneous dynamics are an inherent property attributable to the random assortment of starting coil shapes of different molecules [30].

The appearance of conformation dependent dynamics also influences the mean rate of stretching. While one might expect that in high flow the polymer stretching rate would approach that of the fluid (“affine deformation”), experiments showed that only the initial 25% of the deformation is nearly affine. Beyond this point, the deformation becomes non-affine, due at first to the appearance of hairpin folds and later to the finite extensibility of DNA [28].

Shear flow: Polymer dynamics in shear flow was imaged by Smith, Babcock, and Chu in 1999 [31]. The group's sample cell consisted of a glass top plate and coverslip bottom plate separated by a gap of 50 μm (Fig. 6), a design intended to maximize high-NA imaging quality and shear-rate while minimizing intrusive hydrodynamic surface effects. A motor driving a micrometer screw translated the top plate to create the shear flow, while a second motor moved the entire device in the opposite direction, a technique used to secure consistent imaging of single molecules in their center-of-mass frame.

In a steady shear flow, molecules continually fluctuated between nearly fully coiled and fully stretched conformations while undergoing end-over-end tumbling. A conformational probability distribution revealed that single polymers were almost equally likely to be found at any extension. The fluctuations between conformations were aperiodic and exhibited a power law roll-off at a high frequency, which was attributed to a tumbling instability driven by Brownian motion (Fig. 6). In contrast to the case of extensional flow, the average extension under shear flow was found to increase gradually with increases in the velocity gradient, reaching a plateau below half-full extension.

Additionally, the microscopic and macroscopic responses of DNA solutions were compared by measuring, respectively, polymer extension via fluorescence imaging and bulk viscosity on the same samples (Fig. 7) [32]. Upon starting up a shear flow, an "overshoot" in viscosity occurred prior to an overshoot in extension. This effect was understood as being due to the fact that polymers, which are partly aligned in a direction perpendicular to the flow during early stages of deformation, contribute greater hydrodynamic friction than they do at a later stage when they become strongly aligned in a direction parallel to the flow.

Mixed Flows: In 1974, de Gennes proposed a phase diagram predicting that shear flow was a borderline case for producing polymer extension, and that an abrupt change in behavior, analogous to a phase transition, would occur when the extensional component of the flow exceeded 50% [26]. To test this theory, Babcock *et al.* designed an experiment in which the shear and rotational components of a flow could be adjusted by sliding Teflon rods through grooves of appropriate geometries [33]. While observing the resulting DNA dynamics, they noted that there was, in agreement with de Gennes' phase diagram, a sharp transition in the average equilibrium length when the extensional component exceeded 50%. Additionally, large fluctuations in extension were observed near the critical point of this transition.

2.5 Entangled Polymer Dynamics

Concentrated solutions of polymers exhibit dramatically non-Newtonian behavior because of the high degree of entanglement among polymer chains. For many years the development of a microscopic theory for entangled polymer dynamics remained a puzzle, until de Gennes, Doi, and Edwards developed a revolutionary model describing individual molecules' "reptation" in these solutions [19]. The model posits that the topology of such entangled clusters confines each constituent molecule to a tube-like region parallel to its chain contour, and that these regions demarcate the preferred pathway for any individual molecule to relax: along, and completely within, its theoretical tube. This restricted relaxation was termed "reptation."

Although the reptation model had, by 1994, been successful at predicting many observed properties of concentrated polymer solutions and melts, experimental evidence for tube-like dynamics was still indirect and disputed by some researchers. This uncertainty was largely put to rest through direct imaging of entangled polymer-chain dynamics. Perkins, Smith, and Chu tethered a single, fluorescently-labeled DNA molecule to a 1μm bead, moved the tethered end (via optical tweezers) in a curvilinear path through an entangled solution of unlabeled DNA, and observed the relaxation of the trailing end (Fig 8.) [7]. Above a certain critical concentration (~0.5 mg/ml for lambda phage DNA) the images showed a clear tube-like motion, wherein the trailing end of the stretched molecule would relax exactly along the path traced out by the leading end.

Measurements of the diffusion coefficients of entangled molecules showed that tube-like constraints persisted on time scales long enough to dominate the rate rearrangement of the molecules, and hence the bulk properties of the fluid. The diffusion coefficients also scaled with length and concentration, as predicted by reptation theory.

2.6 DNA Electrophoresis

Gel electrophoresis, one of the most important techniques in molecular biology, separates fragments of DNA by size. The technique allows accurate sizing of DNA molecules ranging from ~10 bp to ~30 kbp by using DC electric fields, and ranging up to the Mbp range by using pulsed electrical fields. In electrophoresis, DNA fragments are driven through porous agarose or polyacrylamide gels, which are known to "sieve" the molecules. Notwithstanding the effectiveness of the widespread biological technique,

however, a complete physical understanding of the mechanisms of this DNA separation is lacking. Developing a better model of electrophoretic separation is of special interest to current efforts to improve the speed and dynamic range of DNA separation, to allow use of smaller sample volumes, and to design independent, microfabricated devices for DNA separation.

Single DNA electrophoretic dynamics: In 1988, J. Deutch presented a series of simulations of the conformational dynamics of single DNA molecules undergoing electrophoresis [34]. In 1989 Smith, and independently, Schwartz and Koval, imaged single DNA molecules by fluorescence microscopy in both DC and pulsed fields in a thin layer of agarose between a slide and coverslip [11,12]. They observed that molecules advanced primarily by lengthwise movement while continually alternating between stretched and contracted conformations, indicating that entropic elasticity and relaxation of DNA play an important role in electrophoresis. In addition, molecules were often observed to get "hooked" on obstacles, causing both ends to temporarily stretch in the direction of the field, forming “U” shapes. More detailed studies were subsequently undertaken by Bustamante and colleagues [35,36]. The behavior of DNA molecules in pulsed field electrophoresis, in which sudden 90° or 120° changes in the field direction are imposed, revealed more complex reorientation dynamics, as shown in Fig. 9.

2.7 Dynamics of DNA Molecules Confined to Two Dimensions

Adsorbed DNA: The restriction that different portions of a polymer chain cannot physically occupy the same space has a much stronger effect on the conformation and dynamics of chains confined to two dimensions than on ones free to move in 3D. The Rouse model reflects this, predicting pronounced distinctions in the dependence of diffusion coefficients upon polymer length for two- and three-dimensionally confined polymers [19].

In 1999, Maier and Radler introduced the elegant technique of binding single DNA molecules electrostatically to a cationic lipid bilayer, creating a surface upon which individual molecules' two-dimensional behavior could be imaged (Fig. 10) [37,38]. As an additional benefit, the high viscosity of the lipid membrane slows molecular conformational dynamics, which improved imaging. Tracking of the Brownian motion of DNA molecules bound in this way revealed that their diffusion coefficient scaled as the inverse of the chain length, as predicted by the Rouse model. Additionally, intra-chain hydrodynamic interactions were found to be negligible due to screening by the lipid layer, confirming a general assumption of the Rouse model. An ensemble of images indicated that the radius of gyration scaled as $L^{1.6}$, in good agreement with a polymeric model based on a two-dimensional, self-avoiding random walk, and in sharp contrast to the $L^{3/5}$ scaling predicted and observed in 3D [19,21]. A reassuring collapse in 2D-molecular size was observed when the concentration of molecules was increased beyond a density at which individual chains would probabilistically overlap. Such a collapse should not -- and in fact does not -- occur in 3D, since the chains can maintain random coil conformations as they entangle, which allows them to occupy large volumes while continuing to avoid one another [19].

Electrophoresis: In 1998, Bakajin *et al*. investigated the electrohydrodynamic stretching of DNA in narrow fluid gaps [39]. Channels with heights ranging from 10 to 0.1 μm were etched in silicon, creating a range of geometries approaching two-dimensionality in which molecular behavior could be observed. Strips of cylindrical posts presented obstacles that transiently stretched molecules in flow. The confined geometry was found first to screen intra-chain hydrodynamic interactions, and second to increase viscous drag, causing DNA to extend more quickly and relax more slowly.

In 2001, Olson *et al*. studied electrophoresis of DNA molecules adsorbed to a cationic lipid bilayer, combining these two previously discussed techniques [40]. Obstacles which caused the DNA to adopt hooked, U-shaped conformations were noted, similar to those observed in 3D electrophoresis (Fig. 11) [Smith, 1989 #71]. Multiple-molecule collisions were observed, but were not sufficiently frequent to be treated by reptation theory. As the electric field was increased, the chains became highly stretched, and their mobility increased significantly. As in the case of DNA in confined channels, the relaxation was slower and the effective hydrodynamic drag was larger than that of free chains.

1.8 Fluorescence Imaging of Protein-DNA Interactions

Binding of proteins to DNA is an integral part of many biochemical processes, and studies of these processes have also benefited from single molecule-fluorescence imaging. In these cases, because the phenomenon of protein-binding casts a protein as the actor and DNA as the acted-upon, it is often more informative to label and image the proteins (rather than the DNA) directly.

RNA Polymerase: Harada *et al*. used total internal reflection fluorescence (TIRF) microscopy to observe RNA polymerase interacting with DNA [41]. In TIRF, molecules near a surface are illuminated by an evanescent wave formed by the total internal reflection of a laser beam, minimizing the amount of stray excitation light reaching the detector and maximizing signal.

In this experiment, a DNA molecule was stretched using optical tweezers over an 8 μm-wide, 2 μm-deep pedestal etched into a glass slide (Fig. 12). This arrangement brought the DNA into the evanescent field, which typically extends only to about ~100 nm within the cell. By observing cy3-labeled RNAp molecules, it became clear that RNAp would bind nonspecifically to any position along the DNA molecule, but that the rate of RNAp's dissociation from the DNA following binding was highly dependent upon its exact position. Encouragingly, dissociation was slower at positions corresponding to known promoter sites (sequences which mark the start of genes to be transcribed, and which thus should distinguish themselves as somehow more "attractive" to RNAp). In contrast to this slow dissociation, RNAp at non-promoter sites was observed to diffuse linearly along the DNA, a process believed to increase RNAp’s ability to find promoter sites quickly. Finally, the overall binding frequency was found to increase with decreasing tension in the DNA.

MuB: Transposition is a form of genetic recombination in which DNA sequences are moved from one site on a genome to another. MuB, a protein coded for by the bacterial virus Mu, is an example of a transposition-facilitating motor, supporting transfer of the viral DNA into a host cell's genome.

Greene and Mizuuchi recently used TIRF to examine formation of the MuB transposition-targeting complex on DNA [42]. First stretching a strand of surface-tethered DNA in flow, and then introducing a solution of green fluorescent protein-labeled MuB to the sample, they observed the formation of large polymeric complexes bound to the AT-rich regions of the DNA. These complexes are believed to serve as targets for DNA strand transfer. A statistical analysis suggested that assembly was initiated by a random nucleation event, and experiments with hydrolyzable and non-hydrolyzable ATP indicated that MuB dissociates from DNA only after hydrolyzing ATP.

2.9 Single Pair Fluorescence Resonance Energy Transfer (spFRET)

Fluorescence Resonance Energy Transfer (FRET) allows detection of conformational changes in macromolecules with resolution far superior to conventional microscopy. In FRET, macromolecules (like DNA) are labeled at two predefined positions with two different dye molecules. Each dye molecule has a fluorescent emission peak that is spectrally distinct from the other's, where the "donor" molecule's emission peak must coincide partly with the excitation peak of the "acceptor." When the donor molecule comes near enough to the other to transfer energy non-radiatively (through an induced-dipole induced-dipole interaction), the acceptor molecule receives this energy and begins to fluoresce at its own emission peak. In addition to this increase in the acceptor's fluorescence, more of the donor molecule's energy is being absorbed into acceptor excitation, its apparent fluorescence is reduced. The efficiency (signal) of a FRET system depends on the inverse-sixth-power of the distance, R, between the donor and acceptor: $E = 1/(1 + (R/R_0)^6)$. R_0 has a typical value of ~5 nm, which means that measurable changes in E occur for molecular movements ranging from ~1 to 10 nm.

The first bulk FRET measurements were performed by Stryer and Haugland in 1967, in which the ends of peptides chains of various length were labeled and the sensitive distance dependence of FRET was observed [43]. More recently, FRET measurements were extended to the single-molecule level, derived from individual biomolecule-labeling by a single pair of donor and acceptor fluorophores, and commonly known as “spFRET” [44]. Either total internal reflection fluorescence microscopy (TIRF) or confocal microscopy can be used to measure spFRET efficiency.

TIRF and Confocal Microscopy: In TIRF, an intensified or cooled CCD camera can image a wide field of view, spanning hundreds of surface-immobilized complexes but currently limited to relatively low frequencies [45]. In confocal microscopy, a laser is focused to a diffraction-limited spot in a sample, and the resulting fluorescence is collected from that region with a photomultiplier tube or an avalanche photodiode, using a pinhole to block stray fluorescence. To form a wide-area image, the stage of the microscope may be raster-scanned over a region of the sample. Alternatively, the laser may be focused into an extremely dilute solution in which individual molecules diffuse in

and out of the excitation volume. This latter configuration is similar to that used in a related technique called fluctuation correlation spectroscopy (FCS) [46].

Diffusing spFRET: In 1999, Weiss and colleagues developed an approach in which confocal spFRET of diffusing molecules is used to infer the distribution of conformations of molecules in solution, compiling denotative histograms of FRET efficiencies from measurements of the bursts of single-molecule fluorescence events (Fig. 13) [47]. In a proof-of-principle study they labeled DNA molecules of various lengths at one end with rhodamine dye and at the other end with Cy5. They demonstrated that subpopulations of different length molecules could be resolved as distinct peaks in FRET efficiency histograms, and that cleavage of a particular DNA molecule by a restriction enzyme could be followed.

Unwinding of DNA by Helicase: Before DNA undergoes replication, the double-stranded molecule must be unwound by helicase enzymes. In 2002, Ha *et al.* used TIRF spFRET to measure the activity of E. Coli Rep Helicase on a single DNA molecule [48]. In this experiment, the two strands at one end of a short dsDNA molecule were labeled with a FRET pair, and the other end of the DNA was attached to a glass slide. Upon unwinding the DNA, the FRET signal was observed to decrease and eventually drop to zero when the strands separated completely. These studies found that a helicase monomer moves toward the ssDNA-dsDNA junction in the presence of ATP, but only unwinds DNA after additional helicase monomers join together to form a complex. Stalls or reversals in unwinding were also observed, suggesting that low unwinding processivity previously observed *in vitro* may be due to instability of the multimeric helicase complex.

3. OPTICAL TWEEZERS

In this section, we provide an introduction to the methods and applications of optical tweezers. We'll begin by explaining the appeal of optical tweezers, give a brief description of the science underlying the phenomenon, describe a variety of basic trap-design considerations, and then track the substantial growth in the biophysical understanding of DNA and related proteins as examples of the experimental sophistication enabled by optical tweezers.

3.1 Motivation: Why "Tweeze"?

Characterizing the mechanical properties of a macroscopic object like a rubber band makes for a pretty simple project: we can see it directly with our eyes, and manipulate it directly with our hands. But when the object we're interested in is somewhere between a million and a billion times smaller than a rubber band, standard measurement devices won't do.

The goal of making mechanical measurements at the microscopic level introduces a host of new experimental considerations, including critical inter- and intramolecular forces, and the appreciable effects of Brownian motion. But since the subject molecules obey the same physical laws as macroscopic objects, there's a special usefulness to

probing the mechanical properties of molecules using basically the same methods that one would apply were the objects a little bigger (or the scientists a little smaller). Experimental elegance aside, there is a simple reason why being able to "grab" a molecule and "pull" on it is appropriate: it is precisely what intuition prescribes. By generating tiny mechanical forces through optical methods, optical tweezers can hold, probe, push, pull, and twist DNA molecules, permitting intuitive interrogation of their mechanical properties.

3.2 Development of Optical Tweezers

The first demonstration of optical tweezers was published in 1970 by Arthur Ashkin. Ashkin arranged a pair of counterpropagating laser beams to come to a common focus in an aqueous sample, generating symmetrical radiation pressures that would "trap" colloidal glass microspheres [49]. Although the paper was a watershed discovery in applied optics, no biological applications were contemplated at the time; Ashkin and colleagues were interested in the trap's applications within physics, and primarily its potential to trap atoms. Sixteen years later -- the same year that the Bell Labs group revolutionized atomic physics by achieving this atom-trapping -- Ashkin, Chu, and colleagues developed a single-laser beam version of the same colloidal-microsphere optical trap, comprising what is now referred to as "optical tweezers." [50]. The interface of tweezers with biology was initiated by Ashkin *et al*.'s 1987 and 1989 publications describing applications of optical trapping for minimally invasive manipulation of viruses, bacteria, and the organelles of protozoa [51,52]. Within a few years, Steve Chu and colleagues were using optical tweezers to manipulate individual DNA molecules [7,15].

3.3 Principles of Optical Tweezers

The operation of modern optical tweezers is often evocative of a curious video game: at the controls, you stare intently into a monitor in which beads in an aqueous well float around, which you grab with invisible laser light and move around carefully with a joystick. In our own lab, the goal of the game is usually to trap two beads with two independently generated tweezers, bump the beads expertly against one another until a single DNA molecule becomes chemically affixed between them, and then turn the controls over to an automatic DNA-stretching machine, which elongates and measures the elastic response of the molecule.

Scientifically speaking, though, the phenomenon that characterizes optical tweezers is the sub-micron precision trapping of glass or plastic microspheres (which range from ~0.1 to 10 μm in diameter) by a laser brought to a tight focus in an aqueous sample-cell. When properly designed optical tweezers are switched on, a microsphere in the vicinity of this focus reacts like a soccer ball rolling to the bottom of a hill, seeking out the lowest-energy position. In the case of a soccer ball, the compelling force is gravity; in the case of optical tweezers, the force arises from the interaction of light with matter. This force can be understood by either classical or quantum mechanical theory [53].

In the classical understanding, a focused laser produces an intense electrical field gradient, which induces a dipole moment in a nearby dielectric sphere. Basic electrostatic theory explains that such dipoles experience a force proportional to the electric field gradient, and thereby move in the direction of maximum field strength. Since the maximum field strength in this case is at the focus of the laser beam, this focus is also the energetic equilibrium point for dipole-carrying microspheres, and serves as the center of the optical trap. Importantly, the more intense and more sharply focused the laser is, the stronger the electric field gradient, and the stronger the optical trap. The classical understanding concludes with the observation that the laser's focus acts like a harmonic potential well for dipoles, meaning that the bead responds as if it were tethered by a Hookean spring to the center of the optical trap.

The quantum mechanical understanding (which admittedly draws on classical optics) regards the laser beam as a stream of photons, carrying momentum equal to Planck's constant divided by the wavelength. Photons incident on a microsphere are either reflected or refracted, and any change in the direction of their propagation may be described as a change in their photonic momentum. By conservation of momentum, the total change in the momentum of incident photons must be balanced by an opposite change in momentum of the sphere: photons reflected back in a direction opposite to the direction of the laser propagation create a so-called "scattering force" or "radiation pressure" that pushes the bead in the direction of the laser propagation, and photons that are refracted through the sphere impart a restoring momentum to the sphere, *opposite* to the direction of the laser's propagation. Although it is counterintuitive that a forward-propagating laser beam could pull a particle backward, conservation of photonic momentum shows this to be a necessary result (see fig. 14). If a laser is strongly focused onto a mostly transmissive sphere, many of the forward-propagating photons are refracted in the *forward* direction, creating momentum transfer that pulls the sphere *back*. The same argument applies to trapping within the focal plane of the laser, where restoring forces opposite to the displacement of microspheres from the trap's center work to hold the sphere in spatial equilibrium.

In general, consideration of the geometry of the photon deflections for various positions of the sphere with respect to the laser beam reveal that the momentum transfer is such that the sphere always tends to be pushed to an equilibrium position slightly beyond the focus of the laser (Fig. 14).

The magnitude of optically generated forces can be estimated by a simple calculation. According to special relativity, the momentum of a photon is given by $p=E/c$. Denoting the initial momentum by $p_0=E/c$ and the final momentum by $p=p_0\theta=E\theta/c$, and then applying conservation of momentum (since the net change in momentum of photons must be equal and opposite to the change in momentum of the sphere that deflected them), we can see that the magnitude of the force acting on the sphere is $F=dp/dt=(dE/dt)\theta/c$. If a 100 mW laser beam, for instance, is focused on a microsphere, and the rays are deflected by the geometrically reasonable angle of milliradians, then the resulting restoring force is within the experimentally verified range of picoNewtons.

3.4 Optical Tweezers Instrumentation

Laser: The first consideration in building optical tweezers is the laser, which must be selected to minimize heating the sample well and the likelihood of damaging biological samples ("opticution," in Ashkin's words). Infrared lasers are a common solution, since most near-infrared radiation is well above the visible-regime absorption peaks in biomolecules and water. Probably the most widely used trapping laser is the Nd:YAG, which operates at 1064nm, although lasers emitting between 800 and 1100nm are usually safe choices [54]. In addition to meeting the wavelength criterion, a single-mode TEM00 laser beam, which is capable of being focused to a small, diffraction limited spot to create a strong trapping potential, is advisable.

Microscope Objective: Because optical tweezers rely on the sharpness of a laser's focus to produce a strong gradient in light intensity, a high numerical aperture (NA) microscope objective is critical to successful tweezer design. The highest relevant numerical aperture objectives are normally 1.4 (for oil-immersion) or 1.2 (for water-immersion). While oil-immersion objectives work well enough in shallow traps, we have found that water-immersion objectives, despite their slightly smaller NA, are much more effective when tweezing deeper than ~10 microns into the sample well for the same reasons that they're often desirable in fluorescence setups: water-immersion lenses correct for the spherical aberrations incurred upon focusing light into an aqueous sample. The resulting tweezers are more apt to exert trapping forces independent of depth in the sample.

Stretching a Single DNA Molecule: To measure the elasticity of DNA—or any linear molecule—only one end of the DNA needs to be mobile, achieving a "stretch" through relative displacement of the two ends.

In a single-tweezer system, one end of a DNA molecule is tethered to a mechanically movable object, and the other to an optically trapped microsphere. Typically, the laser focus will remain fixed, acting as both a trap and a force-measurement device, while the mechanically driven object supplies the necessary stretching force. Wang *et al*., for instance, often elongate DNA between their optical trap and a coverslip, chemically binding to the glass surface by way of a stalled RNAp complex [55]. One single-tweezer setup in our lab employs a glass micropipette to vary the position of a bead attached to one end of the DNA, while a bead attached to the other end is held static in the optical trap [56]. The movable bead remains in static contact with the micropipette because of a strong suction, and the micropipette (and thus bead) position is driven by a piezoelectric nanopositioning stage.

In a dual-tweezer system, both ends of the subject DNA are chemically bound to microspheres, and either one or both of the microspheres may then be optically manipulated to modulate their relative displacement. Traps in a dual-beam system can easily be focused between the bottom and top surfaces of the sample well, a feature that helps reduce undesirable hydrodynamic fluctuations and friction from object-surface interfaces.

The simplest way to create dual traps is to feed a single laser into a polarizing beam-splitting cube, creating two separate optical paths characterized by orthogonal polarizations. Placement of a tip-tilt mirror along one of these paths makes it possible to "steer" the position of that beam, and through proper use of intervening optical elements,

angular movements of this mirror result in pure translational motion along the specimen plane [57]. More complex optical elements, such as acousto-optic deflectors (AODs) or holographic diffraction gratings, can be substituted for the mirror, providing a variety of methods for steering the movable trap.

An intriguing method of producing multiple traps from a single source, "chopping" was first introduced in 1993 by Visscher *et al.* [58,59]. One type of chopping scheme works as follows: an acousto-optic deflector (AOD) receives a single input beam, creates a first-order diffracted beam at an angle, specified by an RF frequency driving the device. This beam, passing through the rest of the optical components leading to the objective and specimen, produces a steerable trap. If the AOD is rapidly chopped between n different frequencies, it will produce n traps at specifiable positions [60]. As far as the mechanics of DNA are concerned, however, tens or hundreds of traps are basically unnecessary; while a phalanx of traps has independent experimental merit, two traps -- for the two ends of DNA -- work just fine.

Measurement of Force and Displacement: Optical tweezers can be configured to measure small forces and displacements with impressive sensitivity [61]. After the end-to-end extension of a DNA molecule is set by positioning the two ends, the tension in the molecule can be determined by measuring the force acting on one of the two attached, optically trapped beads. In general, this force may be measured either by monitoring the displacement of the bead from the center of the trap, or by measuring the deflection of the trapping laser beam. In the former case, the system must first be calibrated to determine the effective spring constant (or "trap stiffness," a figure that is usually given in pN/nm), monitoring the bead position by imaging the bead onto a video camera or, more accurately, a position-sensitive detector. In the latter case, the angular intensity distribution of the laser is monitored by collecting the deflected rays of the trapping laser as they exit the "force-measuring" trapped bead, employing a high-NA condenser and imaging the back focal plane of this condenser onto a position-sensitive detector [62]. Such a system may be calibrated by applying known external forces or by absolute determination of the beam momentum change. In either type of measurement, time-dependent changes in the DNA extension and force, due to protein-DNA interactions for example, can be measured by continual monitoring of the force on the bead.

Several prototypical modes of measurement suit specific experimental goals. In the simplest mode, the trap position is fixed. Changes in elasticity or length of the DNA change the DNA tension, but also result in a slight change in the extension of the DNA due to a shift of position of the bead in the trap with force. In a second mode, the trap position is ramped up and down to cyclically stretch and relax the DNA while the tension is measured. More sophisticated modes involve using feedback to clamp the extension of the DNA or its tension [55,63].

Calibration: Once a working trap exists, it must be calibrated. Calibration comes in two parts: first, calibration of the position of the movable end of the DNA-stretching system with respect to the fixed end, and second, calibration of the displacement force evident from a bead's displacement within the force-measuring trap [64].

Although the centroids of each of a pair of controlled beads can be found with image acquisition software, this is not the most accurate method. Since the measurement is really only relative displacement, two beads can be effectively "zeroed" anew with each experimental run. If a calibrated nano-positioning stage is used to position one end of the DNA (or one bead), the control signal for the stage may be directly taken as specifying the position of that end.

A critical factor in measurement is the ability to relate a trapped microsphere's position within an optical trap to the amount of force pulling it away from the central equilibrium. Several methods of calibration are commonly used, the simplest being a measurement of the trapped microsphere's displacement from the center of the trap by motion of the surrounding fluid (either by moving the bead or producing a steady flow through the sample cell). By balancing the optical restoring force against a displacement force, the latter from Stokes' equation for a viscous suspension and a known bead velocity, the trap's strength and stiffness can be characterized as a function of the bead's displacement from the center [65].

Another commonly used method of calibration draws on the natural Brownian motion of microspheres in solution, invoking the equipartition theorem and determining the trap stiffness κ by the relationship $\frac{1}{2}\kappa\langle x^2\rangle = \frac{1}{2}k_B T$, where k_B is the Boltzmann constant, T the temperature, and $\langle x^2 \rangle$ is the mean-square displacement of the bead from the center of the trap [64].

Finally, now that DNA tension as a function of fractional extension has become well-known through optical measurements, this characteristic elasticity may be used to calibrate the stiffness of optical traps [56].

Attachment of DNA to beads: Biotin and digoxygenin ("dig") labels are usually used to link the ends of DNA to Streptavidin- and anti-dig-coated beads. Several methods may be used for labeling. As lambda DNA has a 12 base single stranded overhang at each end, one may use DNA polymerase to fill in biotin- or dig-labeled nucleotides. To generate molecules with biotin at one end and dig at the other, one can cut a double biotin-labeled molecule using a restriction enzyme to expose fresh overhanging ends, and fill in with dig-labeled nucleotides.

In our lab, we recently developed a general method in which PCR (polymerase chain reaction) is used to label any desired DNA sequence from genomic DNA from any organism by using biotin- and dig-labeled primers. We have used this method to prepare E. coli, drosophila, and human DNA sequences for optical tweezers manipulation.

Alternatively, labeled oligonuclotides (short ssDNA molecules) can be synthesized and ligated (bonded using the enzyme ligase) to the ends of a longer DNA fragment. If only using one biotin or dig label, it is important to realize that these single attachment points are free to swivel. In a case where the attachment needs to be torsionally constrained one may ligate on longer DNA fragments, containing tens or hundreds of labels [66].

3.5 Mechanical Properties of DNA

DNA is a biological polymer which contains the genetic information that propagates characteristics of living organisms across generations of reproduction. DNA forms a double helix with two anti-parallel sugar-phospate backbone chains, held together by hydrogen bonds between complementary nucleotide bases. The crystallographic length of DNA is ~0.34 nm per base pair, and its radial diameter is ~2 nm. Researchers from biology, chemistry, physics, and engineering show a current, evolving interest in understanding the mechanical properties of DNA, but before the advent of single-molecule techniques, interrogation of these properties was limited to the ensemble inferences from bulk-study methods.

Stretching DNA: In 1990, Chu and Kron were the first to apply optical tweezers to manipulate individual DNA molecules [13]. By using polystyrene microspheres as "handles" to which each end of a DNA molecule could be affixed, Chu *et al*. stretched single DNA molecules and observed their entropic relaxation, finding DNA's physical behavior within this low force-extension regime comparable to a Hookean spring, demonstrating a restoring force proportional to the extension from its natural, relaxed state [15]. These early measurements were crude, but they paved the way to more detailed characterizations of dsDNA's elasticity.

Entropic Elasticity: In 1992, the next step was taken by Smith *et al*., who attached a single DNA molecule end-to-end between a slide and paramagnetic bead [18]. By applying a combination of calibrated hydrodynamic and magnetic forces, they stretched the DNA and achieved the first quantitative measurement of the force-extension law for dsDNA. Additionally, they characterized DNA's elasticity under varying concentrations of NaCl and the fluorescence dye ethidium bromide, finding that these reagents did not affect the general form of the force-extension relationship. While Chu's original findings of Hookean behavior in the low-force regime were confirmed, a nonlinear, sharply increasing force-extension relationship was observed for forces above ~1 pN as the extension approached the crystallographic contour length of the DNA. Interestingly, Smith *et al*. showed that the commonly used freely jointed chain (FJC) model of polymer conformation did not fit the data very well (Fig 15).

Subsequent comparison of these data with elasticity calculations for the worm-like chain (WLC) model indicated much better agreement (Fig. 15) [67]. The WLC elasticity, first calculated by Fixman and Kovac [68], assumes that a polymeric molecule is a thin rod with a characteristic stiffness and a continuous curvature, where the magnitude and direction of this curvature are distributed randomly along the infinitesimal segments of the chain [19]. In its natural, relaxed state, dsDNA forms a randomly oriented coil with a characteristic persistence length (a measure of the characteristic length scale on which segments of the molecule to remain correlated, or "persist," in a single direction before becoming uncorrelated). Marko and Siggia revisited this problem in more detail in a 1995 publication in which they introduced an approximate analytic formula for the inextensible WLC elasticity as follows:

$$F = \left(\frac{kT}{P}\right)\left[\frac{1}{4(1-x/L)^2} - \frac{1}{4} + \frac{x}{L}\right]$$

where kT is the thermal energy, P the persistence length, x the end-to-end extension, and L the contour length of the polymer [69]. Fitting the elasticity data to the WLC model yielded a persistence length of 53.2 ± 2.3 nm in 10 mM NaCl, which was consistent with previous estimates from bulk studies [67].

Deforming DNA: In 1996, Smith *et al*. made DNA elasticity measurements at higher forces by developing a new optical tweezers apparatus and introducing several novel techniques to refine their measurements [56]. Their most important contribution to optical tweezing was the direct measurement of the change in the laser momentum to infer the force acting on the trapped bead. Using a dual-beam trap symmetrically positioned around a common focus within a sample well -- it was similar to Ashkin's original apparatus in this respect -- a single trap was created at the center of the two objectives. During an experiment, this single trap would hold one bead, again bound chemically to one end of a DNA molecule, while the molecule's other end would be held by suction to the tip of a mechanically positioned micropipette (Fig. 16)

Smith *et al*. also developed an elegant procedure for attaching a single DNA molecule, biotinylated at each end, between two streptavidin beads as illustrated in Fig. 16. The optical trap was first used to catch a bead and place it on the tip of a micropipette. A flow of dilute DNA was introduced such that a DNA molecule was captured onto this bead. Typically the DNA was found to bind by only one end while the other end stretched in the flow due to hydrodynamic drag. A second streptavidin bead was then trapped and brought near the extended end of the DNA to form an attachment. Upon confirming that the two beads were linked by the spanning piece of DNA -- apparent from a visible mechanical coupling of the two -- the micropipette was gradually translated back and forth to stretch and relax the DNA. Measurement of the relative position of the beads was determined by video imaging, and measurement of the bead's displacement from the center of the optical trap was determined by deflection of the trapping laser beam by position-sensitive photodetectors located strategically behind each objective (Fig. 16).

Under applied forces of <10 pN, the dsDNA exhibited behavior similar to what had been seen in previous studies, yielding results in agreement with the WLC-model. Between ~10 and 60 pN, however, the elasticity changed and a linear enthalpic-stretching term was needed to account for stretching of the DNA slightly beyond its crystallographic contour length. This behavior was first modeled by Odijk, who gave the following formula for DNA elasticity in the high force (greater than few pN) limit:

$$x = L\left[1 - \frac{1}{2}\left(\frac{kT}{FP}\right)^{1/2} + \frac{F}{S}\right]$$

where S is the stretch modulus [70]. The data fit quite well to this expression, yielding S=1000 pN in a buffer solution containing 150 mM NaCl.

Overstretching DNA: At ~65 pN (in a high salt of ~150 mM NaCl), an unexpected structural transition was observed: the DNA stretched to about 1.7 times its normal crystallographic contour length while asserting only 2 pN of additional resistance (Fig. 17) [56,71]. This transition was termed "overstretching." Upon relaxation, a dsDNA molecule exhibited some hysteresis in the force-extension behavior, attributed to force-induced partial "melting" of the double-stranded DNA into two single strands.

Single-stranded DNA (ssDNA) molecules were also stretched using the tweezer apparatus, revealing a dramatically different contour length and flexibility than observed for dsDNA (Fig 18). Prior to these measurements it had often been assumed that ssDNA, being highly flexible, could probably be modeled using the FJC model. However, data were not fit very well by this model, particularly at high force. Instead, a modified FJC model incorporating an elastic stretch term gave a much better fit, yielding values of 0.75 nm for the persistence length and an 800 pN stretch modulus [56]. No overstretching transition was observed for ssDNA. The measured length of ssDNA in the asymptotic high force limit was similar to that of fully overstretched DNA, suggesting that overstretching may represent unwinding of the two strands to form a fully base-paired parallel ladder.

Using an optical tweezers apparatus based on the design of Smith *et al.*, Bloomfield and colleagues studied the dependence of dsDNA overstretching on temperature, pH, and ionic strength [72]. On the basis of these measurements they proposed a model that postulates that the overstretching transition corresponds to force-induced melting of the dsDNA. Calculations of the predicted effect of temperature, pH, and salt in their model were found to agree well with measured overstretching forces. They observed that pH values outside the range from 5 to 9, increases in temperature from 20 to 50 degrees C, or decrease in the monovalent salt concentration from 1000 to 2.6 mM, reduced the force needed to overstretch. Such dependence on NaCl had also been reported by Smith *et al.* (Fig. 19) [56]. To reconcile their model with the observation that the two strands of the overstretched DNA do separate at the end of the overstretching transition, they proposed that fully overstretched DNA was being mostly melted but contained a small number of "helical domain boundaries" which held the strands together, as opposed to the fully base-paired ladder form suggested by Smith *et al*.

High Precision Measurements: In 1997, Wang *et al.* performed DNA elasticity measurements using an optical tweezers apparatus with improved sensitivity (Fig 20) [55]. They implemented a "position-clamp" which held the bead at a fixed position in the trap, allowing accurate determination of force-extension data without needing to correct for changes in extension due to displacement of the bead in the trap.

Single DNA molecules were attached by one end to a slide and by the other end to an optically trapped bead. The molecule was stretched by translating the stage with respect to the fixed optical trap, and the position of the bead in the trap was measured using interferometry [Denk, 1990 #145]. The force was calculated by multiplying the bead displacement by the calibrated trap stiffness. Once the measured force reached a particular level corresponding to a specified extension of the DNA a feedback loop that modulated the intensity of the trapping beam via an acousto-optic modulator was

activated in order to maintain a constant bead position in the trap. Modulating the intensity of the trap-forming beam produced a corresponding change in the trap-stiffness. Their high resolution data in the force range from 0.1 to 50 pN confirmed the appropriateness of the WLC model yielding a persistence length of 47 nm and stretch modulus of ~1100 pN in a buffer containing 10 mM NaCl.

Force Fluctuations in DNA: Pressing the previous standards of sensitivity in optical tweezers measurements, Meiners and Quake recorded the Brownian force fluctuations of a DNA stretched between two optically trapped beads in order to characterize the relaxation time of a stretched polymer [73]. DNA was held at fractional extensions ranging from 0.72 to 0.92 and computation of the cross-correlation averaged over several minutes allowed characterization of force fluctuations at sensitivity levels down to ~6 femtonewtons rms (Fig 21). Two beams having orthogonal polarizations were used to create the two traps and independently detect bead displacements. They also found it necessary to chop the traps alternately at high speed (80 kHz) in order to reduce cross-talk between the two detectors. Interestingly, the transverse and longitudinal relaxation times were observed to split into two distinct values, in agreement with predictions based on the differences in hydrodynamic drag for chain segments moving perpendicular or parallel to the chain contour.

It should be noted that the high force fluctuation sensitivity achieved in this experiment derives from being able to compute an averaged cross-correlation function from several minutes of recorded data. Unfortunately, this technique does not provide femtonewton resolution to static forces or transient force changes, but only to RMS values of steady state force fluctuations.

Unzipping the double helix: Extending DNA manipulation techniques even further in 1997, Heslot and colleagues introduced a method for unzipping (separating) the two strands of the double helix [74,75]. Their initial measurements employed a flexible microneedle as a force transducer, but then in 2002 they improved their experimental resolution by using optical tweezers. The two strands were pulled apart as shown in Fig. 22. They found that the measured force signal was dependent on the local sequence of the DNA being unzipped, with as sections of higher G-C content required higher forces to unzip than sections containing higher A-T content.

While this method was thought to hold potential as a technique for sequencing single DNA molecules, experiments have only been able to resolve sequence features down to the ten base pair scale. Also, measurements indicated that thermal equilibrium is not always reached, even at the lowest pulling rates studied (20 nm/s). Flipping of the force signal between discrete levels was observed and interpreted as being due to transitions between different minima in a complex energy landscape. Therefore, while some improvements in resolution could still be achieved by reducing instrumental noise and drift, it is unclear whether unzipping will ever allow determination of DNA sequence at the single-molecule level.

Twisting DNA: A method for twisting a single DNA molecule was first introduced by Strick *et al*. in 1996 [66]. Following the scheme introduced by Smith *et al*., they attached

a single DNA between a surface and a magnetic bead. They then used a rotating magnet to both twist and stretch the DNA, revealing that the elasticity of DNA changes dramatically with applied twist. Later, several other groups incorporated DNA twisting into their experiments. In 1999 Leger *et al*. attached one end of a DNA molecule to a bead held by a micropipette on a rotary mount and the other end to a thin optical fiber acting as a force-transducing cantilever [76]. An important finding of this experiment was that torsionally constrained, untwisted DNA overstretches at ~110 pN as opposed to the value of ~65 pN for unconstrained DNA.

In 2003, Bryant *et al*. introduced a new method for measuring torque on a single DNA held stretched using optical tweezers [77]. In their experiment, one end of the DNA was attached in a torsionally constrained way to a bead on a micropipette while the other end was attached to a bead in an optical trap. As in the experiment of Leger *et al*., the micropipette was rotated to twist the DNA. A third bead was attached to the side of the DNA at a point between the two ends, allowing the torsional relaxation of the DNA against a defined torque produced by hydrodynamic drag to be observed by watching the attached bead spin as the DNA relaxed. Measurements of the torque as a function of twist allowed them to determine a torsional modulus of ~400 pN nm^2, a more accurate value than was possible using traditional bulk measurements. Several structural transitions were also observed to occur in force-torque phase space.

3.6 Protein-DNA Interactions

Methods to measure DNA elasticity have also been applied to study protein-DNA interactions, a topic of special interest to molecular biology. This section presents a modest, illustrative selection of such tweezer-based studies.

Chromatin: The DNA of humans and other higher organisms is stored in the form of a protein-DNA complex called chromatin. Chromatin plays an important role in gene storage, permitting single cells to contain several-meter lengths of DNA by employing a series of molecular spools around which such enormous lengths of DNA are wound and compressed to occupy a space only a few microns in diameter.

The fundamental subunit of chromatin is the nucleosome, a core octomer of histone proteins bound to a ~150 bp segment of a long strand of DNA. Because the DNA is wound, rather than elongated, this structure shortens the end-to-end extension of the DNA dramatically. This makes it ideal not only for biological packaging, but also for interrogation by optical tweezers.

Initial chromatin-stretching studies were performed by Cui and Bustamante, who used chromatin harvested from chicken erythrocytes [78]. They observed continuous deformation of the molecules at low forces and in low salt concentrations, inferring a persistence length of ~30 nm and stretch modulus of ~5 pN. For higher salt concentrations (~100 mM NaCl), they observed a force plateau at ~5 pN, attributed to disruptions of internucleosomal interactions. After applying stretching forces of >20 pN, they observed a marked hysteresis during relaxation of the molecules, interpreted as a signature of irreversible unbinding of histones. By elongating the spooled molecules, they

were likely "popping" off the histone octamers that form the spooled structure of chromatin, creating an unspooled molecule exhibiting the elasticity of naked dsDNA.

Subsequent work by Brower-Toland *et al*. examined a homogeneous preparation of periodic nucleosome arrays assembled onto a periodic DNA template by salt dialysis, whereby an adiabatic change from high to low salt "anneals" histones onto the subject DNA [79]. They observed gradual unfolding at low forces followed by a "sawtooth" pattern in the force vs. extension data, where the sawteeth were ascribed to the unravelling of individual nucleosomes (Fig. 23). These abrupt events occurred at forces of 20-30 pN, and were measured to release ~80 bp of DNA with each removed nucleosome.

Bennink *et al*. had also witnessed a sawtooth pattern in an earlier study, using optical tweezers and a flow cell to assemble chromatin-like molecules *in situ* [80]. By flowing cell extracts past a tethered DNA molecule, the group observed that the molecule would compact against the direction of the flow, and inferred the selective binding of nucleosomes to segments of the DNA. Upon controlled elongation, sudden sawtooth-like changes in length of the DNA by ~380 bp and ~190 bp were frequently observed.

Interestingly, though, these changes are larger than the ~145 bp length of DNA demonstrated as present in crystallographic nucleosome structures, suggesting either that the measurement could not resolve the finer details seen by Brower-Toland *et al*., or that the *in situ*-derived chromatin was not well-formed. Subsequent measurements in our lab (unpublished data) on nucleosome arrays assembled *in vitro* using purified Drosophila histones, the chaperone protein NAP-1, and ACF (ATP-dependent chromatin assembly factor) have shown abrupt unravelling events most frequently releasing ~80 bp per event, in good agreement with the findings of Brower-Toland *et al*.

RecA: RecA is a protein that mediates the swapping of one strand between two double-stranded molecules in bacterial recombination and DNA repair. The polymerization of RecA protein on DNA has been studied by Hegner *et al.* and Shivashankar *et al.* using optical tweezers [81,82], revealing that when RecA is polymerized onto the DNA, the resulting fiber is about 50% longer than naked DNA, and that the subject DNA's persistence length and stretch modulus increase. In the presence of ATP, the fiber length was found to be unstable, switching between polymerization at ~12 monomers/s and depolymerization at ~2 monomers/s. In the presence of a non-hydrolyzable ATP analog, the length was found to be more stable and the stretch modulus increased by a factor of two, indicating tighter RecA binding in the ATP-bound state.

3.7 DNA translocating molecular motors

There is great current interest among biophysicists in biomolecular processes involving "molecular motors," enzymes that convert chemical energy into observable mechanical work. While the longest-studied and most thoroughly explored of these motor proteins is myosin [Mehta, 1999 #146] (the complex that generates the force and movement responsible for muscle contractions), we limit our discussion here to a several examples of DNA-related motors.

RNA Polymerase: One of the most important processes in biochemistry is the transcription of DNA sequences into RNA, a process catalyzed by the enzyme RNA Polymerase (RNAp).

In 1995, Yin *et al*. introduced an optical tweezers assay for studying the force and movement of an individual RNAp protein as it moves along a DNA molecule [83]. In this assay, stalled RNAp-DNA complexes -- stalled because they were deprived of the necessary physiological concentrations of deoxy-nucleotides (dNTPs) and pyrophosphate (PPi) -- are adsorbed onto a glass slide, and a 0.5 μm bead is attached to the downstream, biotinylated end of the DNA. The bead is optically trapped and repositioned to hold the DNA under a small amount of measured tension. The RNAp begins to reel in the tethered bead, asserting a gradually increasing force as it pulls the bead further from the center of the trap, and the position of the bead is measured with nanometer resolution using interferometry [Denk, 1990 #145].

Interestingly, RNAp was found to stall at an average resistive force of 14 pN, several times larger than that myosin's stall force (~3 pN). Measurements of mechanical work, when compared to the free energy available from the motor's estimated rate of hydrolysis of its "fuel" adenine triphosphate (ATP), suggested an apparent energy conversion efficiency of ~10-20%.

In subsequent experiments optical tweezers employing the intensity-modulating force-feedback scheme described above were developed to control trap stiffness dynamically, and thus to maintain a constant bead position against RNAp's translocating force (Fig. 24) [84]. Such "isometric" measurements eliminate the need to correct force data for finite compliance of the linkages (including DNA, RNAp, and interfaces between these and the bead), which can be advantageous in situations where the compliance is unknown, or the force is changing rapidly.

Measurement of the velocity as a function of force indicated that rate-limiting biochemical steps at low force-loads did not generate movement, and that high resistive loads may stall RNAp by sliding the enzyme backwards along the DNA by 5-10 bp, an unexpectedly large molecular distance. Pauses in transcription were observed and found to be independent of the applied load, indicating that they were not due to RNAp backtracking, as had been suggested previously. The data suggest that these pauses, instead, are caused by a structural change in the enzyme.

DNA Polymerase: DNA replication is a fundamental biological process in which genetic information is copied, driven by the enzyme DNA polymerase. In 2001, Wuite *et al*. studied the single-molecule mechanics of replication by stretching a single-stranded DNA molecule between two optically trapped beads and measuring the change in its elasticity as it was converted, via T7 DNAp, to double-stranded form [85]. As shown in Fig. 25, under applied tensions of <6.5 pN, the end-to-end distance of ssDNA is shorter than that of dsDNA, which allows continuous measurement of the progress of DNAp under a constant load.

DNAp moved most quickly (~200 bp/s) when the DNA tension was 5 pN, exhibiting slower rates at both lower and higher tensions. These data were interpreted by comparing the measured mechanical work done with predictions of a model for mechanical and entropic work done by the enzyme, suggesting that DNAp organizes two bases in the

polymerase site during each catalytic cycle. T7 DNAp is also known to contain an exonuclease (nucleotide removing) activity localized in a different domain of the enzyme. In optical tweezers experiments, this activity was found to be enhanced by 100-fold when tensions above 40 pN were applied to the DNA, suggesting that this tension reorients the enzyme, facilitating the exonuclease site's interaction with the DNA.

Viral DNA Packaging: The packaging of DNA into a pre-formed viral capsid (a protein shell) is a critical step in viral assembly. Viral molecular motors powered by ATP hydrolysis aim to "package" DNA within empty capsids, drawing the biomolecules through a ~3 nm diameter portal in the capsid.

To explore the mechanics of this viral molecular motor, Smith *et al*. created a stalled, partly packaged bacteriophage phi29-DNA complex and attached these to streptavidin-coated microspheres via a terminal biotin on the DNA (see fig. 26) [86]. A single microsphere was trapped and brought in contact with a second microsphere coated with anti-prohead antibodies and held by suction on the end of a micropipette, forming a stable tether. Data on the force generation and DNA translocation were recorded in one of two modes: in the first mode, the DNA tension was allowed to build as the packaging proceeded, allowing measurement of the force-velocity relationship and stall force of the motor; in the second mode, feedback was used to maintain a constant tension of ~5 pN as the DNA was translocated by controlling the pipette position with a piezoelectric stage.

Impressively, the motor was found to exert forces of up to ~70 pN on the DNA, making phi29 one of the strongest known biological motors. The maximum rate of packaging in saturating ATP was found to be ~100 bp/s; once the prohead had become mroe than 50% full, the packaging rate began to drop, approaching zero as the ~6 μm long viral genome neared full packaging.

Comparison of these data with the force-velocity relationship measured under an external load suggests that an electrostatic counter-force builds within the capsid during packaging, consistent with theoretical estimates of the energy required to confine the negatively charged DNA to the small, ~50 nm diameter space of the prohead. Integration of the force-distance relationship allowed calculation of the mechanical work done, and indicated a chemical-to-mechanical energy conversion efficiency of ~30%.

References

1. Larson R. G. (1998) *The Structure and Rheology of Complex Fluids*, Oxford University Press.
2. Klotz L. C., Zimm B. H. (1972) *J Mol Biol* **72**, 779.
3. Haugland R. P. (2004)
4. http://www.microscopyu.com/articles/formulas/formulasresolution.html
5. Schnapp B. J., Gelles J., Sheetz M. P. (1988) *Cell Motil Cytoskeleton* **10**, 47.
6. Yildiz A., Forkey J. N., McKinney S. A., Ha T., Goldman Y. E., Selvin P. R. (2003) *Science* **300**, 2061.
7. Perkins T. T., Smith D. E., Chu S. (1994) *Science* **264**, 819.
8. Morikawa K., Yanagida M. (1981) *J Biochem (Tokyo)* **89**, 693.
9. Matsumoto S., Morikawa K., Yanagida M. (1981) *J Mol Biol* **152**, 501.

10. Yanagida M., Hiraoka Y., Katsura I. (1983) *Cold Spring Harb Symp Quant Biol* **47 Pt 1**, 177.
11. Smith S. B., Aldridge P. K., Callis J. B. (1989) *Science* **243**, 203.
12. Schwartz D. C., Koval M. (1989) *Nature* **338**, 520.
13. Chu S., Kron, S. (1990) *Int. Quantum Electron. Conf. Tech. Digest (Optical Society of America, Washington DC, 1990)* 202.
14. Kasevich *et al.* M. (1991) *AIP Conf. Proc.* **233**, 47.
15. Chu S. (1991) *Science* **253**, 861.
16. Perkins T. T., Quake S. R., Smith D. E., Chu S. (1994) *Science* **264**, 822.
17. Bustamante C. (1991) *Annu Rev Biophys Biophys Chem* **20**, 415.
18. Smith S. B., Finzi L., Bustamante C. (1992) *Science* **258**, 1122.
19. Doi M., Edwards S. (1987) *The Theory of Polymer Dynamics*, Oxford University Press.
20. Matsumoto *et al.* M. (1992) *J Polym Sci Pol Phys Ed.* **30**, 779.
21. Smith D., Perkins T., Chu S. (1996) *Macromolecules* **29**, 1372.
22. Perkins T. T., Smith D. E., Larson R. G., Chu S. (1995) *Science* **268**, 83.
23. Larson R., Perkins T., Smith D., Chu S. (1997) *Phys Rev E* **55**, 1794.
24. de Gennes P. G. (1979) *Scaling Concepts in Polymer Physics*, Cornell University Press.
25. Quake S., Babcock H., Chu S. (1997) *Nature* **388**, 151.
26. de Gennes P. G. (1974) *J. Chem. Phys.* **60**, 158.
27. Perkins T., Smith D., Chu S. (1997) *Science* **276**, 2016.
28. Smith D., Chu S. (1998) *Science* **281**, 1335.
29. Schroeder C., Babcock H., Shaqfeh E., Chu S. (2003) *Science* **301**, 1515.
30. Larson R. G., Hu H., Smith D. E., Chu S. (1999) *J. Rheology* **43**, 267.
31. Smith D. E., Babcock H. P., Chu S. (1999) *Science* **283**, 1724.
32. Babcock H. P., Smith D. E., Hur J. S., Shaqfeh E. S., Chu S. (2000) *Phys Rev Lett* **85**, 2018.
33. Babcock H., Teixeira R., Hur J., Shaqfeh E., Chu S. (2003) *Macromolecules* **36**, 4544.
34. Deutsch J. M. (1988) *Science* **240**, 922.
35. Gurrieri S., Rizzarelli E., Beach D., Bustamante C. (1990) *Biochemistry* **29**, 3396.
36. Gurrieri S., Smith S. B., Wells K. S., Johnson I. D., Bustamante C. (1996) *Nucleic Acids Res* **24**, 4759.
37. Maier B., Radler J. (1999) *Phys Rev Lett* **82**, 1911.
38. Maier B., Radler J. (2000) *Macromolecules* **33**, 7185.
39. Bakajin O., Duke T., Chou C., Chan S., Austin R., Cox E. (1998) *Phys Rev Lett* **80**, 2737.
40. Olson D., Johnson J., Patel P., Shaqfeh E., Boxer S., Fuller G. (2001) *Langmuir* **17**, 7396.
41. Harada Y., Funatsu T., Murakami K., Nonoyama Y., Ishihama A., Yanagida T. (1999) *Biophys J* **76**, 709.
42. Greene E., Mizuuchi K. (2004) *J Biol Chem* **279**, 16736.
43. Stryer L., Haugland R. P. (1967) *Proc Natl Acad Sci U S A* **58**, 719.
44. Ha T., Enderle T., Ogletree D., Chemla D., Selvin P., Weiss S. (1996) *Proc Natl Acad Sci U S A* **93**, 6264.
45. Ha T. (2001) *Methods* **25**, 78.
46. Haustein E., Schwille P. (2003) *Methods* **29**, 153.

47. Deniz A., Dahan M., Grunwell J., Ha T., Faulhaber A., Chemla D., Weiss S., Schultz P. (1999) *Proc Natl Acad Sci U S A* **96**, 3670.
48. Ha T., Rasnik I., Cheng W., Babcock H. P., Gauss G. H., Lohman T. M., Chu S. (2002) *Nature* **419**, 638.
49. Ashkin A. (1970) *Phys. Rev. Lett.* **24**, 156–159.
50. Ashkin A., Dziedzic J., Bjorkholm J., Chu S. (1986) *Optics Letters* **11**, 288.
51. Ashkin A., Dziedzic J. M. (1987) *Science* **235**, 1517.
52. Ashkin A., Dziedzic J. M. (1989) *Proc Natl Acad Sci U S A* **86**, 7914.
53. Ashkin A. (1992) *Biophys. J.* **61**, 569.
54. Neuman K. C., Chadd E. H., Liou G. F., Bergman K., Block S. M. (1999) *Biophys J* **77**, 2856.
55. Wang M., Yin H., Landick R., Gelles J., Block S. (1997) *Biophys J* **72**, 1335.
56. Smith S., Cui Y., Bustamante C. (1996) *Science* **271**, 795.
57. Fallman E., Axner O. (1997) *Appl Optics* **36**, 2107.
58. Visscher K., Brakenhoff G., Krol J. (1993) *Cytometry* **14**, 105.
59. Visscher K., Gross S., Block S. (1996) *IEEE J Sel Top Quant* **2**, 1066.
60. Molloy J. E. (1998) *Methods Cell Biol* **55**, 205.
61. Lang M. J., Asbury C. L., Shaevitz J. W., Block S. M. (2002) *Biophys J* **83**, 491.
62. Gittes F., Schmidt C. (1998) *Biophys J* **74**, A183.
63. Visscher K., Block S. M. (1998) *Meths. Enzymol.* **298**, 460.
64. Svoboda K., Block S. M. (1994) *Annu Rev Biophys Biomol Struct* **23**, 247.
65. Simmons R. M., Finer J. T., Chu S., Spudich J. A. (1996) *Biophys J* **70**, 1813.
66. Strick T. R., Allemand J. F., Bensimon D., Bensimon A., Croquette V. (1996) *Science* **271**, 1835.
67. Bustamante C., Marko J. F., Siggia E. D., Smith S. (1994) *Science* **265**, 1599.
68. Fixman M., and Kovac, J. (1973) *J. Chem. Phys.* **58**, 1564.
69. Marko J., Siggia E. (1995) *Macromolecules* **28**, 8759.
70. Odijk T. (1995) *Macromolecules* **28**, 7016.
71. Cluzel P., Lebrun A., Heller C., Lavery R., Viovy J., Chatenay D., Caron F. (1996) *Science* **271**, 792.
72. Williams M., Rouzina I., Bloomfield V. (2002) *Accounts Chem Res* **35**, 159.
73. Meiners J. C., Quake S. R. (2000) *Phys Rev Lett* **84**, 5014.
74. Essevaz Roulet B., Bockelmann U., Heslot F. (1997) *Proc Natl Acad Sci U S A* **94**, 11935.
75. Bockelmann U., Thomen P., Essevaz-Roulet B., Viasnoff V., Heslot F. (2002) *Biophys J* **82**, 1537.
76. Leger J., Romano G., Sarkar A., Robert J., Bourdieu L., Chatenay D., Marko J. (1999) *Phys Rev Lett* **83**, 1066.
77. Bryant Z., Stone M., Gore J., Smith S., Cozzarelli N., Bustamante C. (2003) *Nature* **424**, 338.
78. Cui Y., Smith S., Bustamante C. (1998) *Biophys J* **74**, A230.
79. Brower-Toland B. D., Smith C. L., Yeh R. C., Lis J. T., Peterson C. L., Wang M. D. (2002) *Proc Natl Acad Sci U S A* **99**, 1960.
80. Bennink M., Leuba S., Leno G., Zlatanova J., de Grooth B., Greve J. (2001) *Nature Struc Biol* **8**, 606.
81. Hegner M., Smith S., Bustamante C. (1999) *Proc Natl Acad Sci U S A* **96**, 10109.
82. Shivashankar G., Feingold M., Krichevsky O., Libchaber A. (1999) *Proc Natl Acad Sci U S A* **96**, 7916.

83. Yin H., Wang M. D., Svoboda K., Landick R., Block S. M., Gelles J. (1995) *Science* **270**, 1653.
84. Wang M., Schnitzer M., Yin H., Landick R., Gelles J., Block S. (1998) *Science* **282**, 902.
85. Wuite G. J., Smith S. B., Young M., Keller D., Bustamante C. (2000) *Nature* **404**, 103.
86. Smith D., Tans S., Smith S., Grimes S., Anderson D., Bustamante C. (2001) *Nature* **413**, 748.

Fig. 1

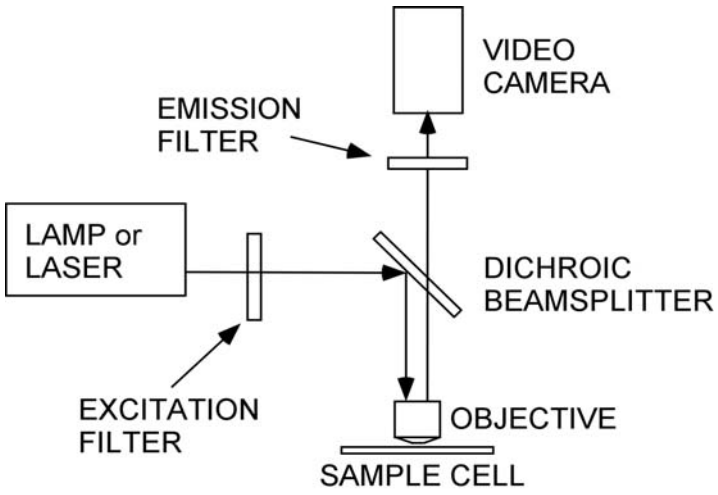

Fig. 1. Schematic of a typical epifluorescence microscopy setup.

Fig. 2

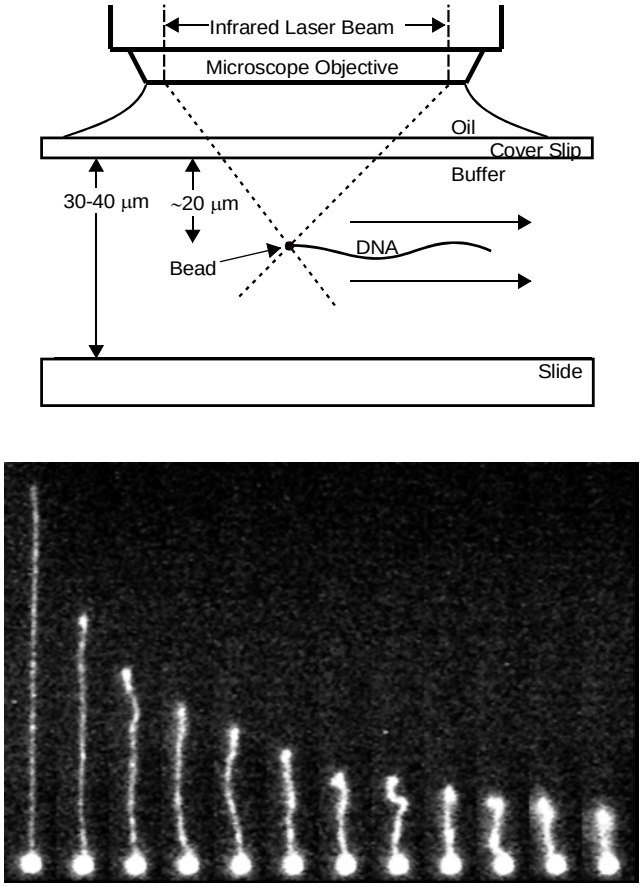

Fig. 2. Manipulation and visualization of a single DNA molecule using optical tweezers and fluorescence microscopy. Top: Schematic of setup. Bottom: Time series of images of a ~40 mm long DNA molecule relaxing after being stretched out in a fluid flow. Reproduced with permission from *Science* 264, 822 (1994)

Fig. 3

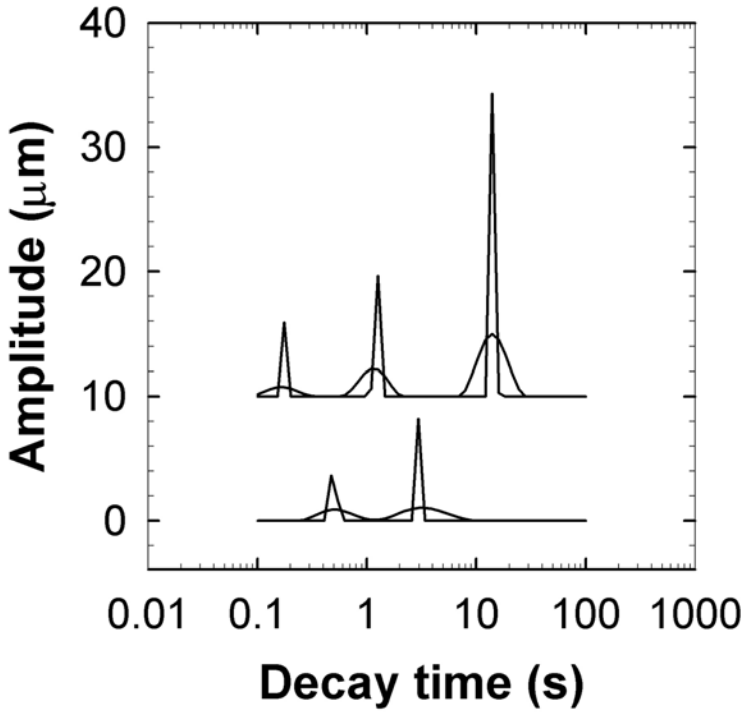

Fig. 3. Relaxation spectra determined by inverse Laplace transform of the extension vs. time relaxation data for single DNA molecules. Top curves are for a ~38 mm long molecule, bottom curves are for a ~13 mm long molecule. Pairs of curves correspond to range of solutions consistent with the experimental data. Reproduced with permission from *Science* 264, 822 (1994).

Fig. 4

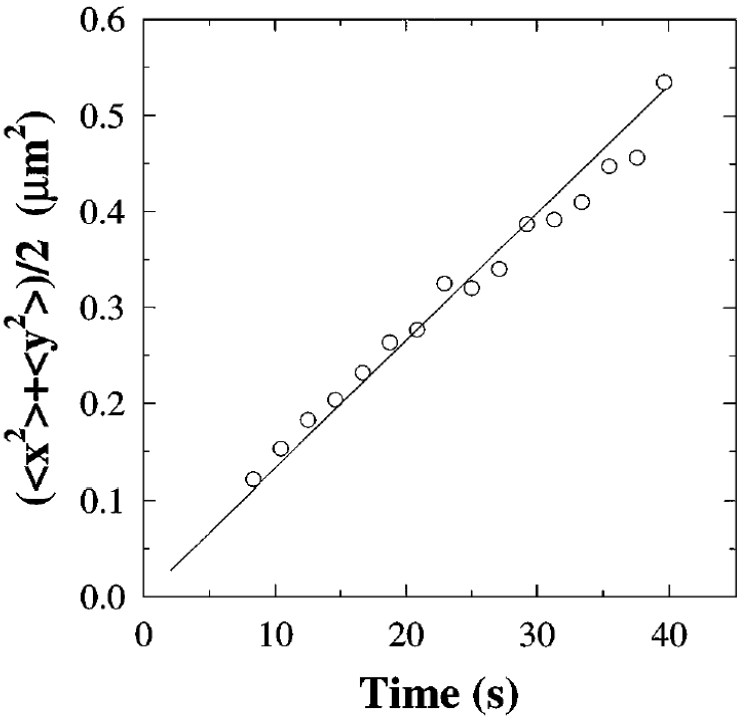

Fig. 4. Mean-square displacement versus time for a diffusing lambda phage DNA molecule determined by tracking the Brownian motion of the centroid with fluorescence microscopy. The slope of the fitted line yields the diffusion coefficient. Reproduced with permission from *Phys Rev Lett* **75**, 4146 (1995).

Fig. 5

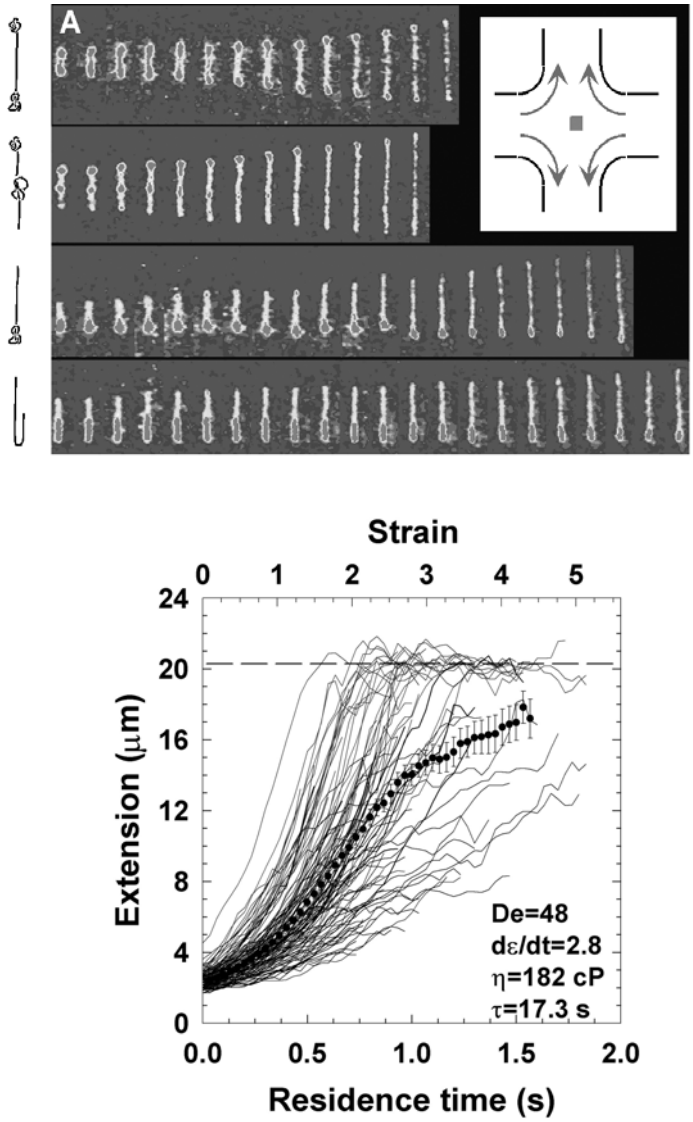

Fig. 5. Top: Stretched lambda DNA molecules in an extensional flow exhibit different types of transient conformations. Bottom: extension data recorded for a large number of identical molecules in identical flow conditions, revealing "molecular individualism." Top reproduced with permission from *Science* **276**, 2016 (1997). Bottom reproduced with permission from *Science* **281**, 1335 (1998).

Fig. 6

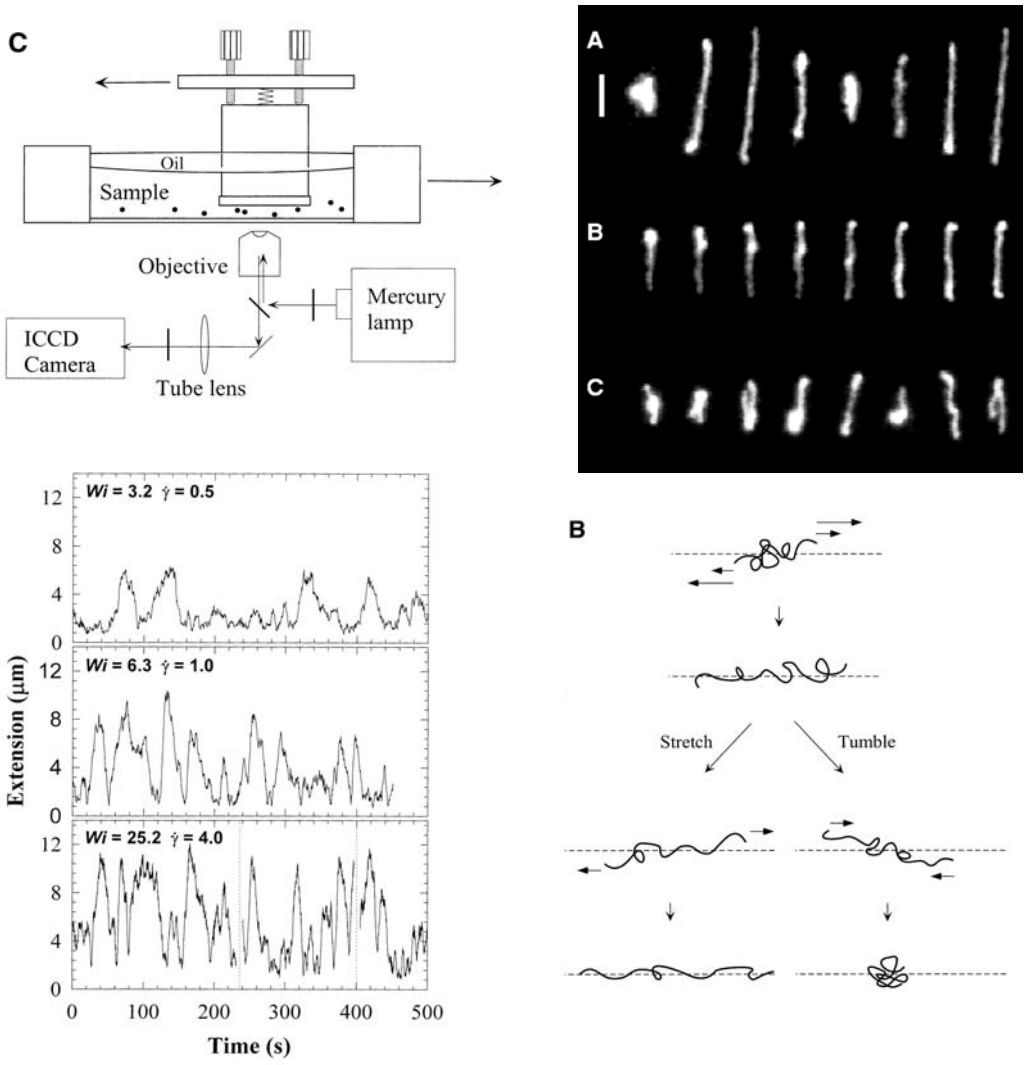

Fig. 6. Top left: Schematic of shear flow apparatus used to image single molecules in their center-of-mass reference frame. Top right: Images of the temporal dynamics of a single lambda DNA molecule in shear flow. Bottom left: Extension fluctuations for various shear rates. Bottom right: cartoon model of the Brownian tumbling instability that causes molecules in shear flow to stretch and contract erratically. Reproduced with permission from *Science* **283**, 1724 (1999).

Fig. 7

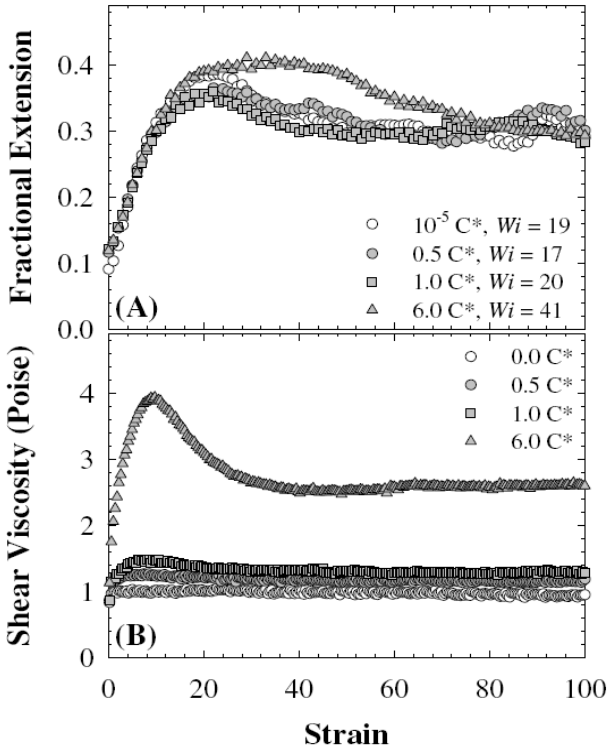

Fig. 7. Comparison of extension observed by fluorescence microscopy (top) versus viscosity (bottom) during the start up of shear flow. *Wi* referrs to the Weissenberg number, which is equal to shear rate multiplied by polymer relaxation time. The concentration is given as factors of C*, which is the threshold concentration for coil overlap. Reproduced with permission from *Phys Rev Lett* **85**, 2018 (2000).

Fig. 8

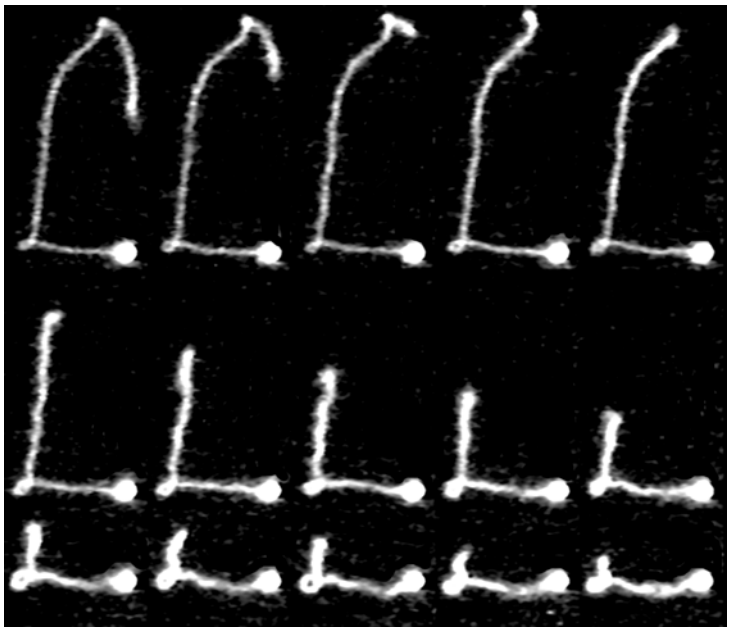

Fig. 8. A series of images over a period of two minutes showing the tube-like motion of a 100 mm-long fluorescently labeled DNA stretched by optical tweezers and relaxing in a 0.6 mg/ml of unlabeled DNA. Reproduced with permission from *Science* **264**, 819 (1994).

Fig. 9

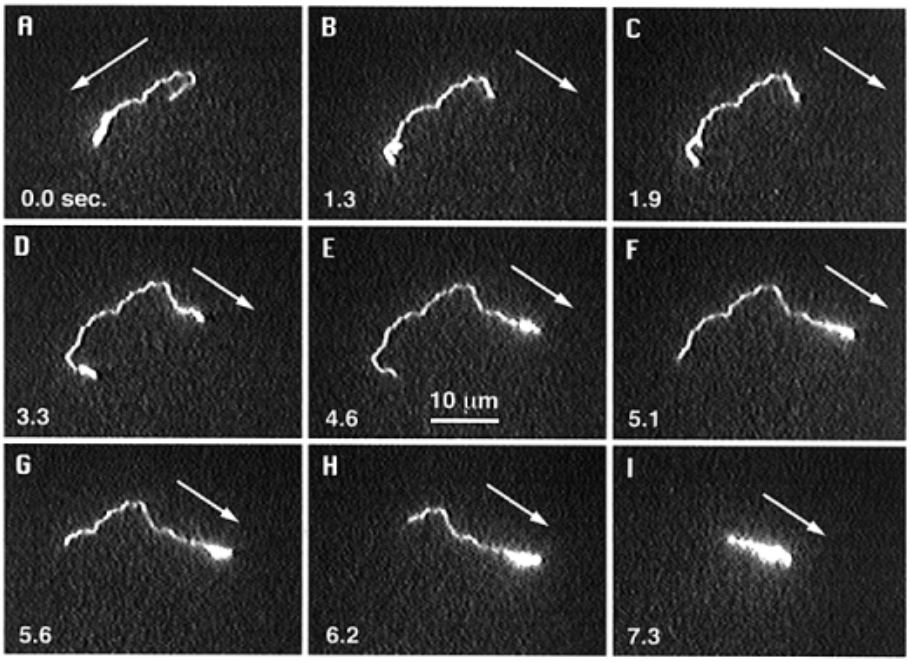

Fig. 9. Reorientation dynamics of a single T2 phage DNA molecule during 120º pulsed field electrophoresis. Reproduced with permission from *Nucleic Acids Res* **24**, 4759 (1996).

Fig. 10

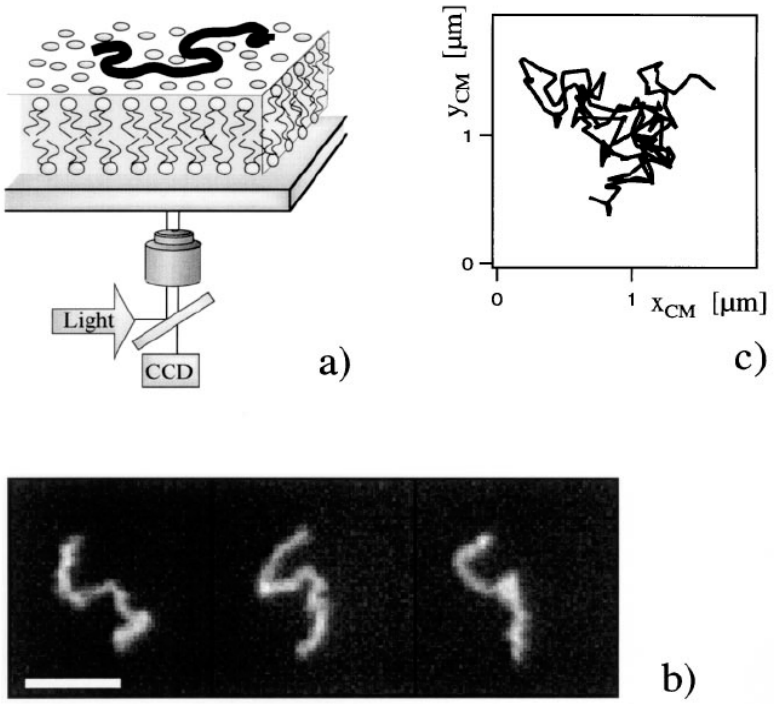

Fig. 10. Fluorescence imaging of the conformation and dynamics of a lambda phage molecule adsorbed to on a 2D cationic lipid bilayer. (a) Schematic of apparatus. (b) Cypical fluorescence images. (c) Tracking of the molecule's centroid during Brownian motion. Reproduced with permission from *Macromolecules* **33**, 7185 (2000).

Fig. 11

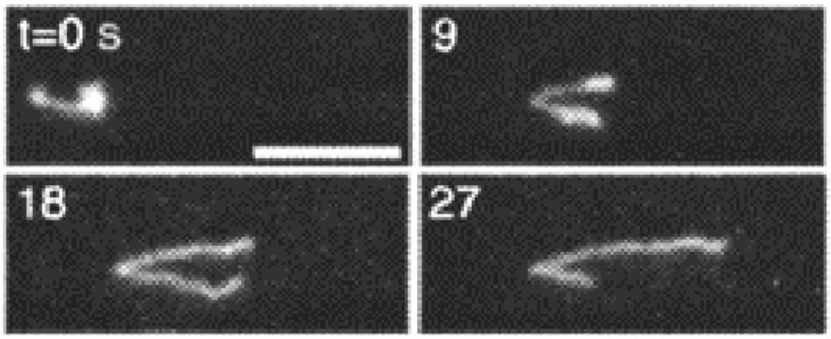

Fig. 11. Fluorescence imaging of the hooking of a lambda DNA molecule on an invisible obstacle while adsorbed on a 2D lipid bilayer during electrophoresis. Reproduced with permission from *Langmuir* **17**, 7396 (2001).

Fig. 12

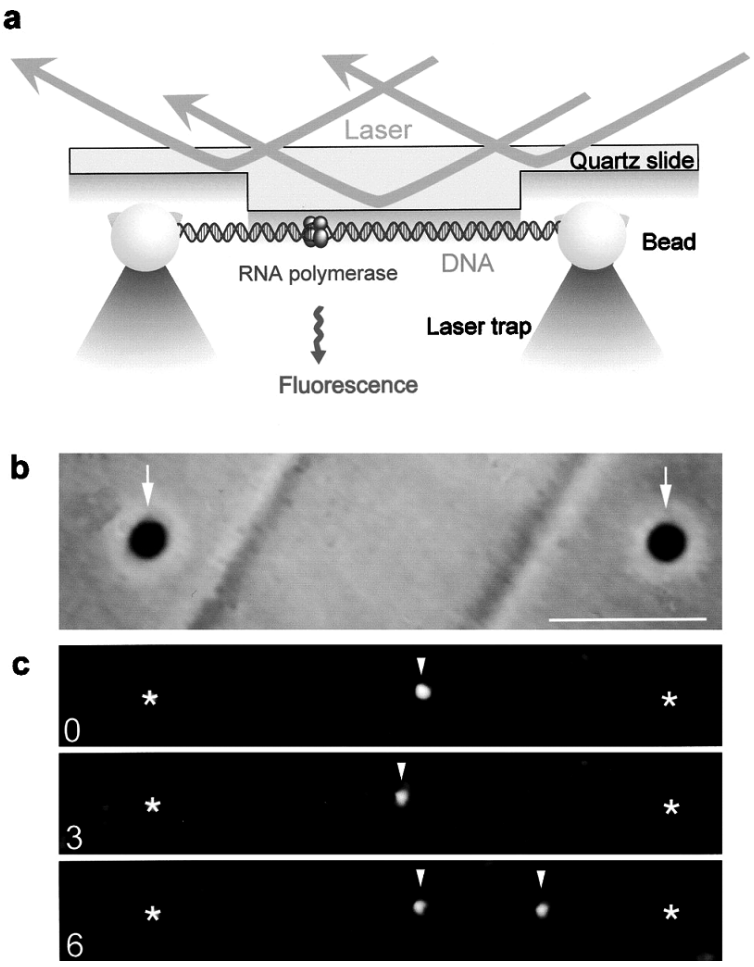

Fig. 12. Total internal reflection fluorescence imaging of single cy3-labeled RNA polymerase molecules binding to a single lambda DNA molecule held stretched by optical tweezers. (a) Schematic of experiment. (b) Brightfield images showing beads and pedestal in glass surface. (c) Fluorescence images showing RNAp binding. Reproduced with permission from *Biophys J* **76**, 709 (1999).

Fig. 13

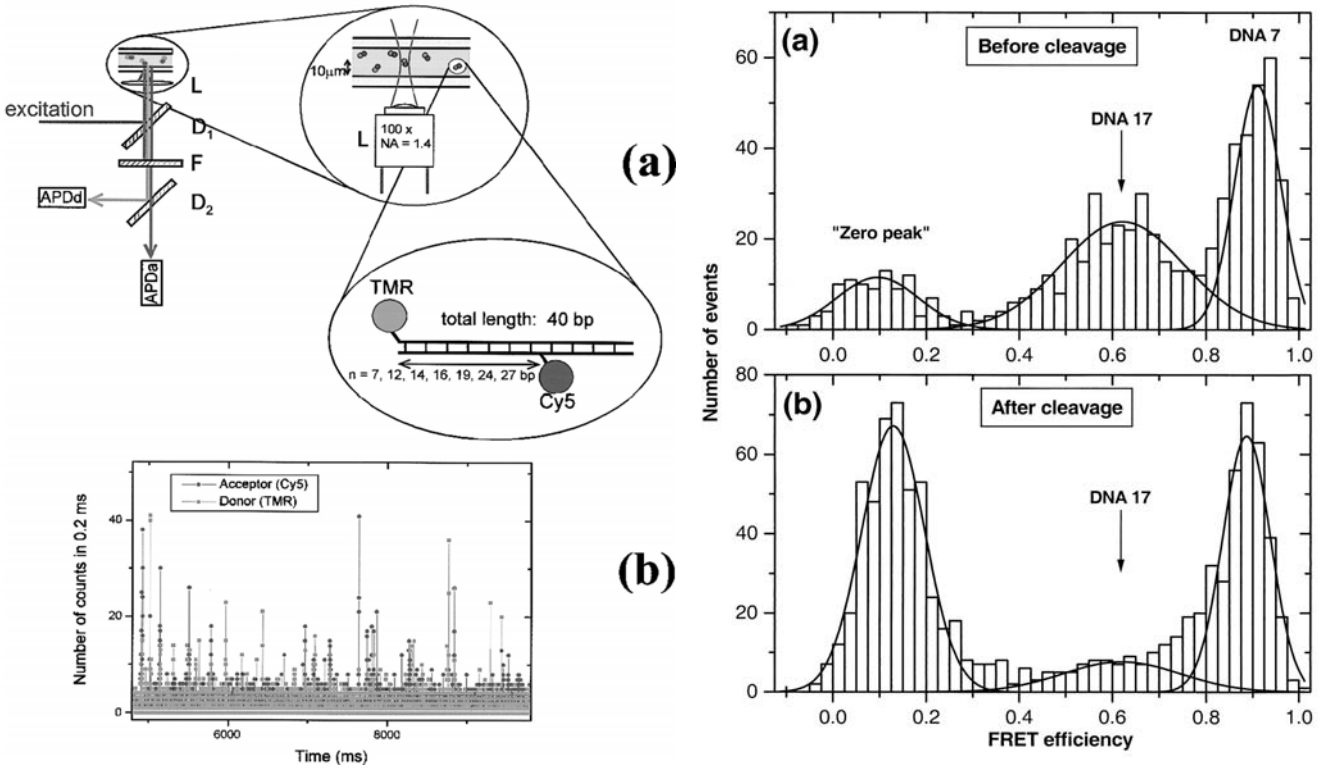

Fig. 13. Fluorescence resonance energy transfer (FRET) measurements between a single donor-acceptor pair of dyes attached to a single DNA molecule. Top left: Schematic of the confocal microscope apparatus in which donor and acceptor fluorescence is recorded from single diffusing molecules. Bottom left: Photon counts vs. time showing spikes, as single molecules diffuse into and out of excitation volume. Top right: FRET efficiency histograms for a mixed ensemble of 7 and 17 bp DNA molecules, showing peaks corresponding to subpopulations. Bottom right: Reduction in peak corresponding to 17 bp DNA upon specific cleavage with a restriction endonuclease. Reproduced with permission from *Proc Natl Acad Sci USA* **96**, 3670 (1999).

Fig. 14

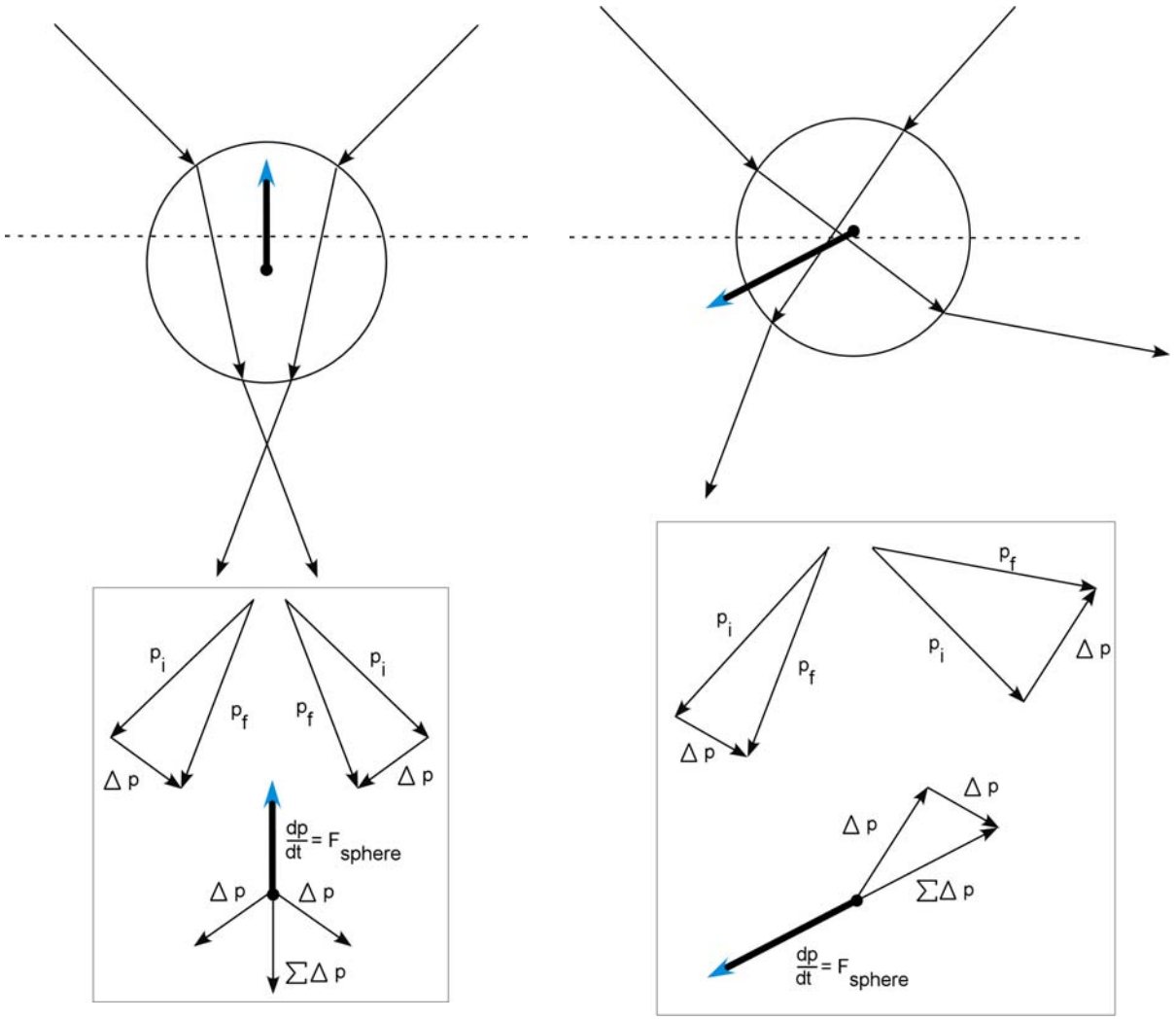

Fig. 14. A ray-tracing model of the gradient force underlying optical tweezers. Left: the microsphere is slightly beyond the trapping beam's focus, so it incurs a restoring force from incident rays in the direction opposite to the beam's propagation. This gradient force is balanced against a scattering force which pushes the bead in the beam direction (back scattered rays not shown). Right: a lateral offset results in the bead being driven toward the trap's central equilibrium point.

Fig. 15

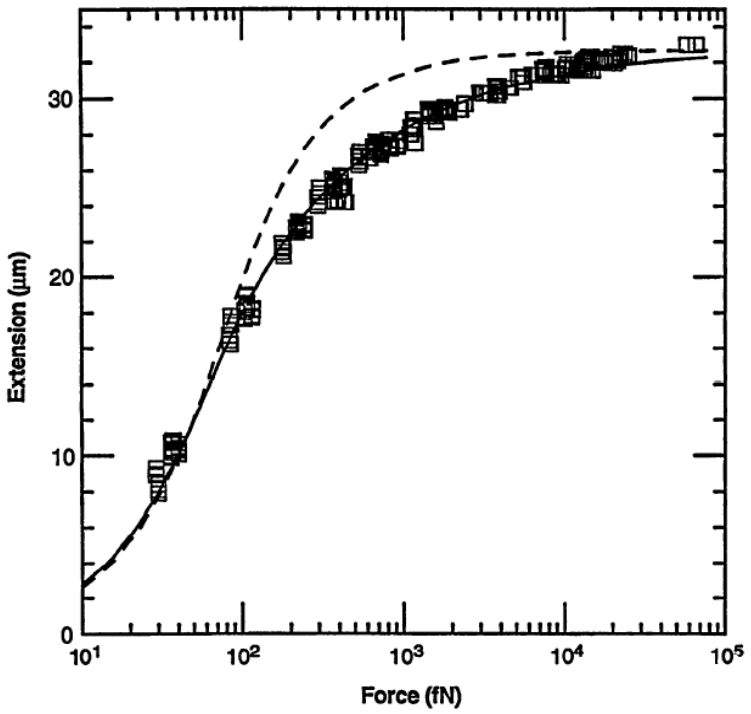

Fig. 15. Single DNA elasticity fit by the worm-like chain model (solid line) and freely jointed chain model (dashed line). Reproduced with permission from *Science* **265**, 1599 (1994).

Fig. 16

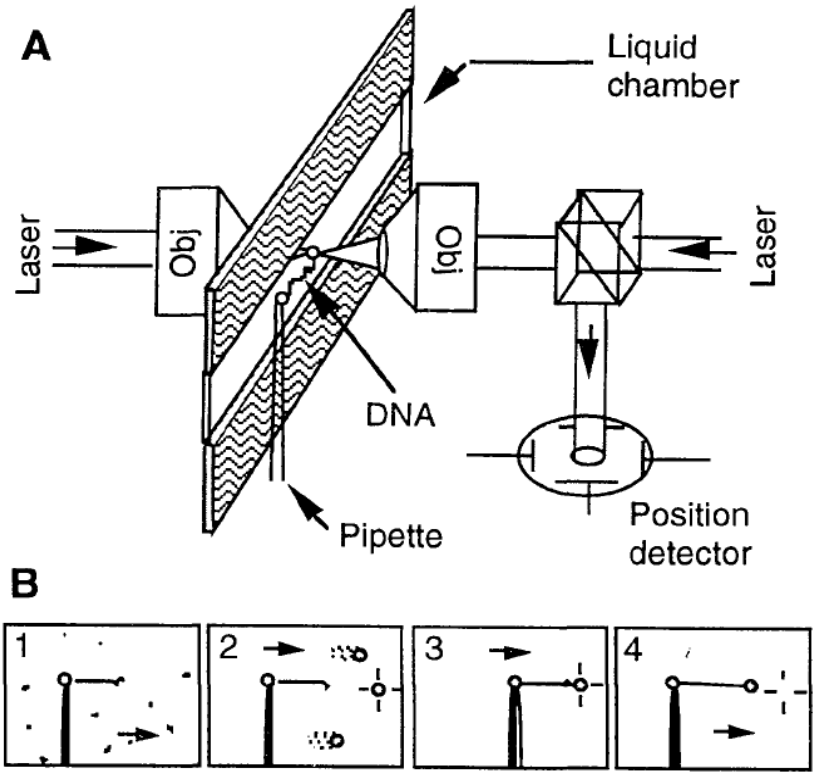

Fig. 16 (A) Setup of a dual-beam, force-measuring optical tweezers used to measure the elasticity of single DNA molecules. (B) Cartoon of method used to tether a single DNA molecule between two beads. Reproduced with permission from *Science* **271**, 795 (1996).

Fig. 17

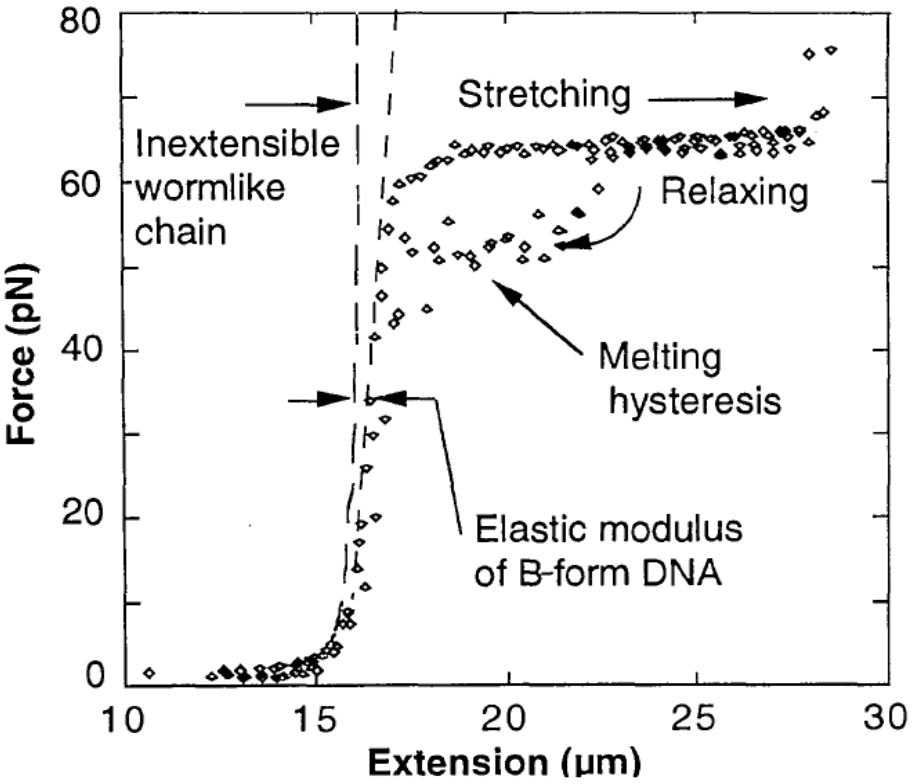

Fig. 17. Measurement of the force-extension behavior of a single dsDNA molecule, showing the entropic and enthalpic portions and the overstretching transition. Reproduced with permission from *Science* **271**, 795 (1996).

Fig. 18

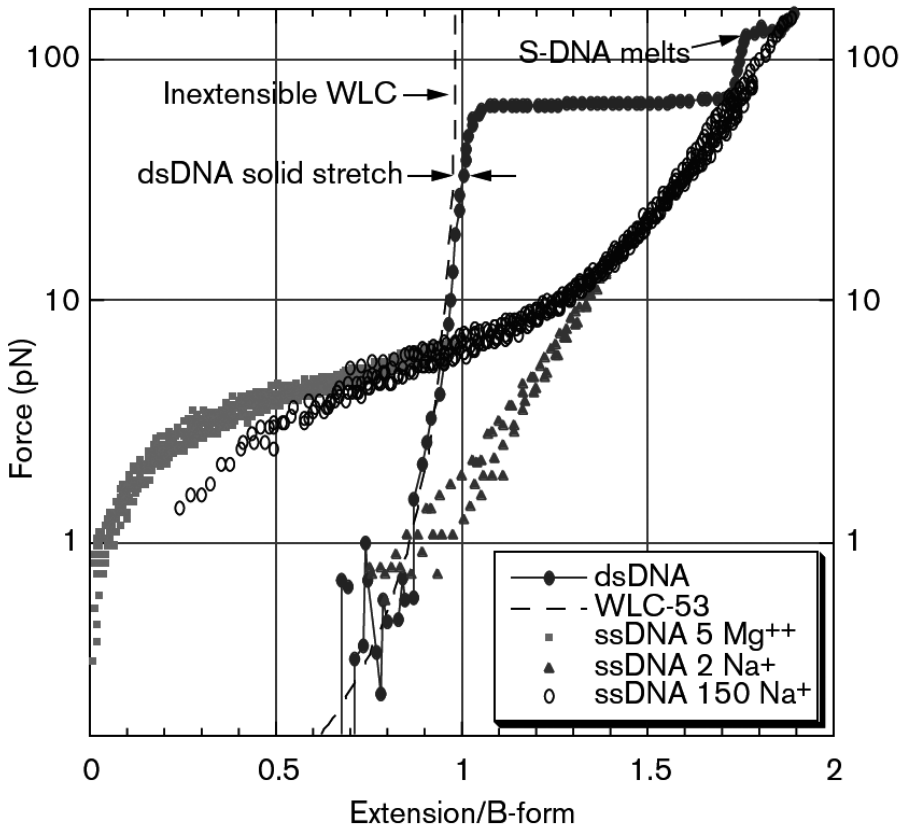

Fig. 18. Elasticity measurements on double-stranded and single-stranded DNA compared with the inextensible worm-like chain model. Reproduced with permission from *Curr Opin Struc Biol* **10**, 279 (2000).

Fig. 19

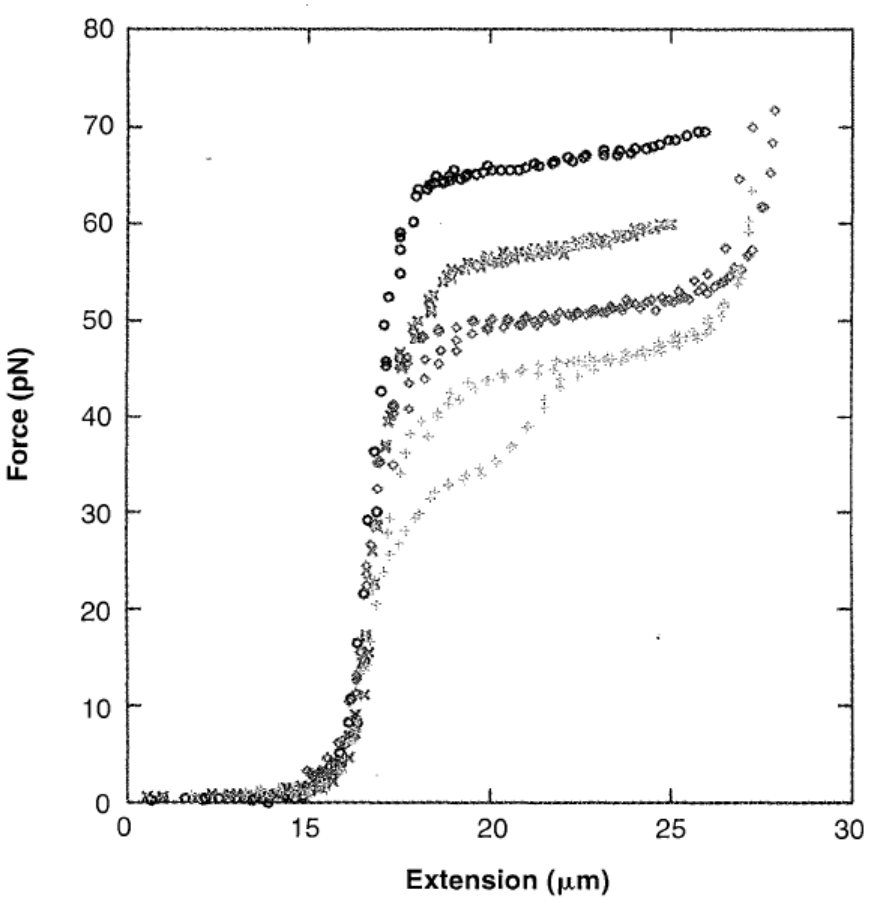

Fig. 19. Dependence of the overstretching transition on NaCl. Reproduced with permission from *Science* **271**, 795 (1996).

Fig. 20

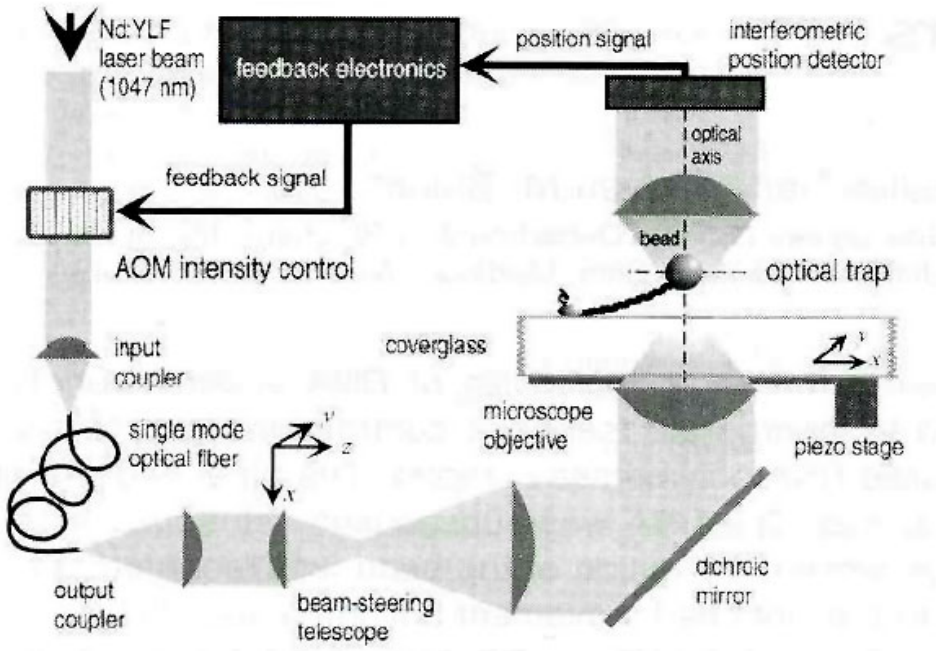

Fig. 20. Schematic of optical tweezers setup used for stretching DNA with optical tweezers, employing feedback to clamp the position of the bead during force measurement. Reproduced with permission from *Biophys J* **72**, 1335 (1997).

Fig. 21

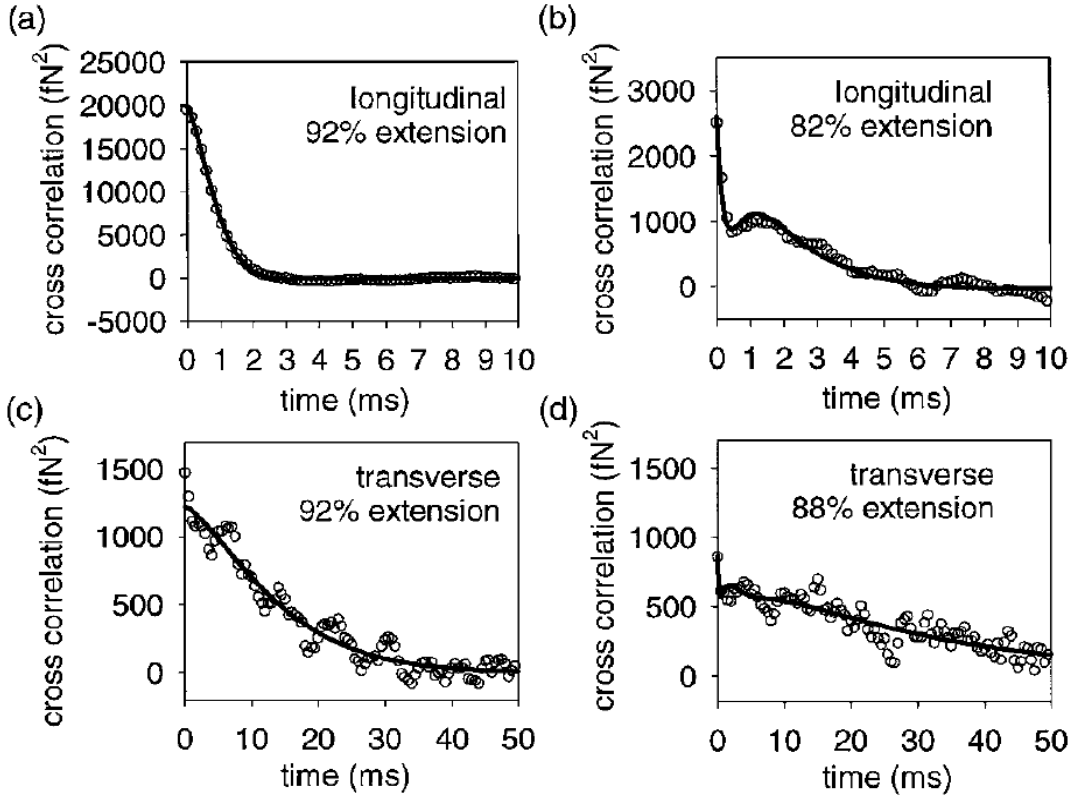

Fig. 21. Cross-correlations of the transverse and longitudinal force fluctuations of beads attached at both ends of a single DNA molecule stretched to various extensions. Reproduced with permission from *Phys Rev Lett* **84**, 5014 (2000).

Fig. 22

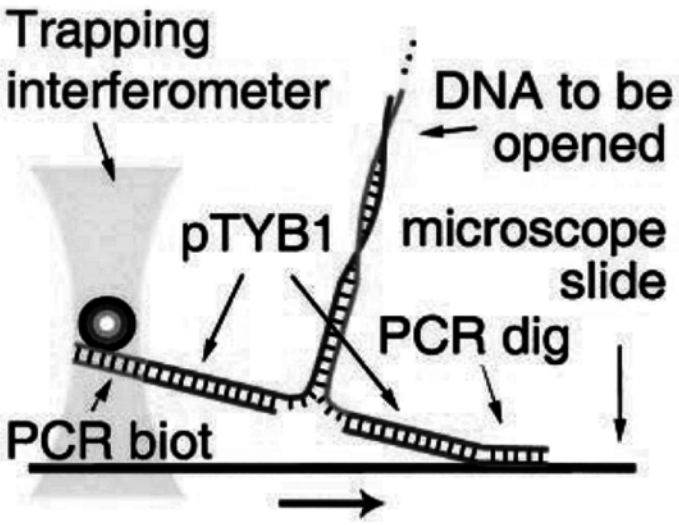

Fig. 22. Schematic of arrangement used to unzip the two strands of a double stranded DNA molecule. Reproduced with permission from *Biophys J* **82**, 1537 (2002).

Fig. 23

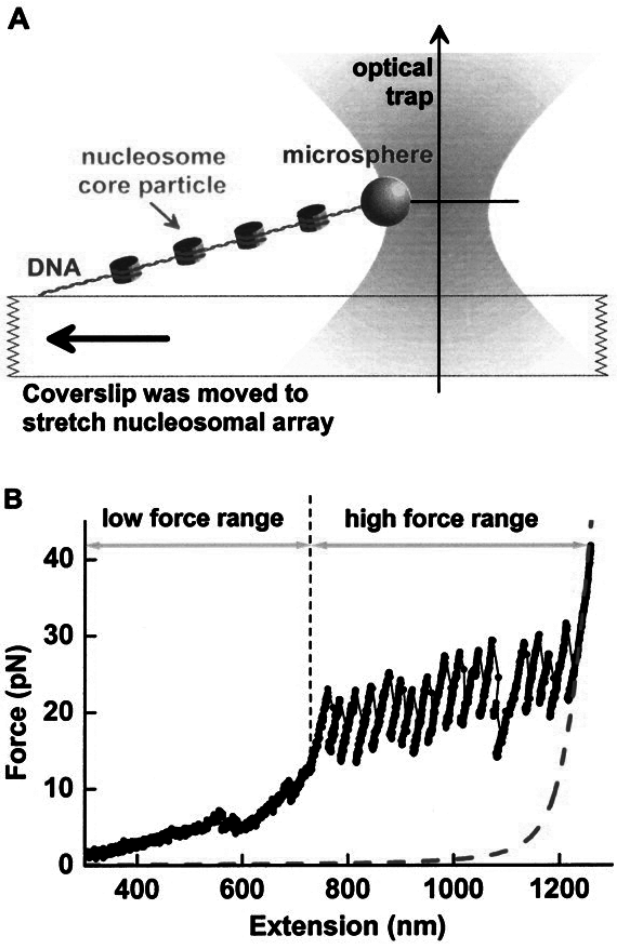

Fig. 23. Schematic of setup used to measure nucleosome unraveling (A) and force-extension data (B). Reprinted with permission from *Proc Natl Acad Sci USA* **99**, 1960 (2002).

Fig. 24

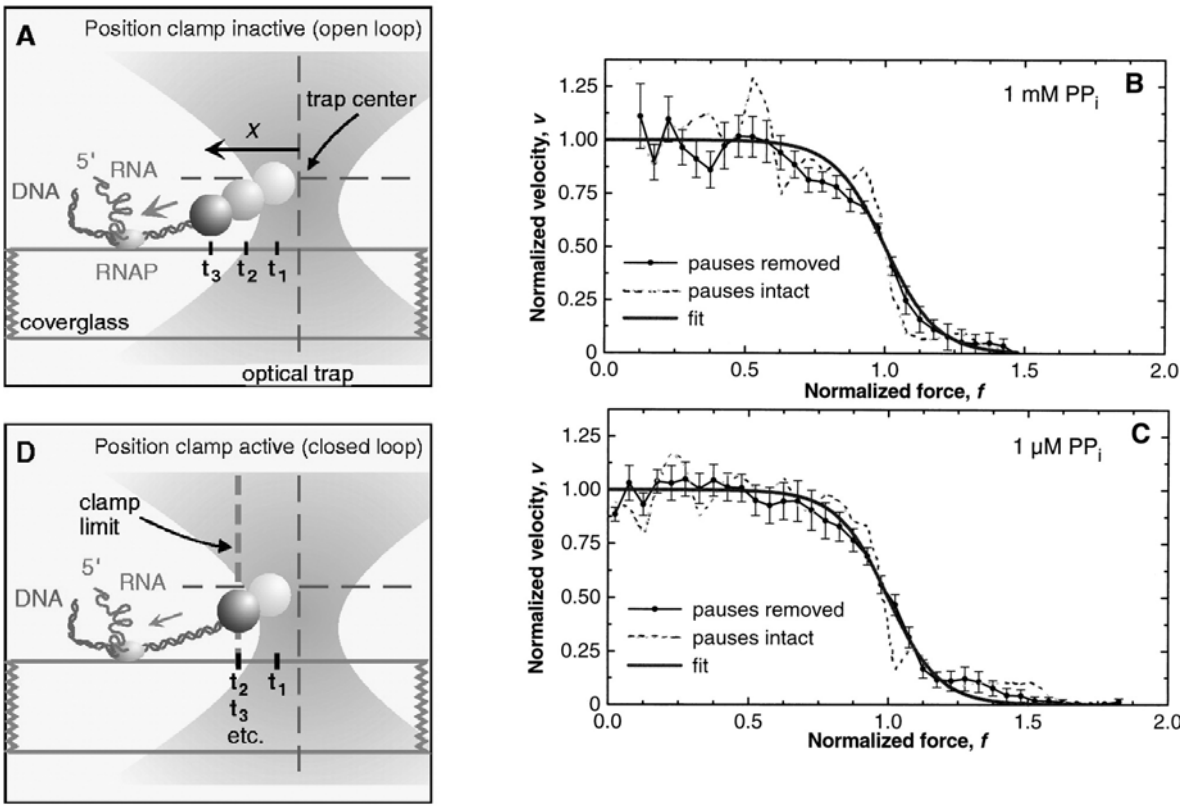

Fig. 24. Measurements of transcription by single RNA polymerase molecules. (A + D) Experimental setup for position clamp measurements. (B + C) Velocity vs. load force data. Reprinted with permission from *Science* **282**, 902 (1998).

Fig. 25

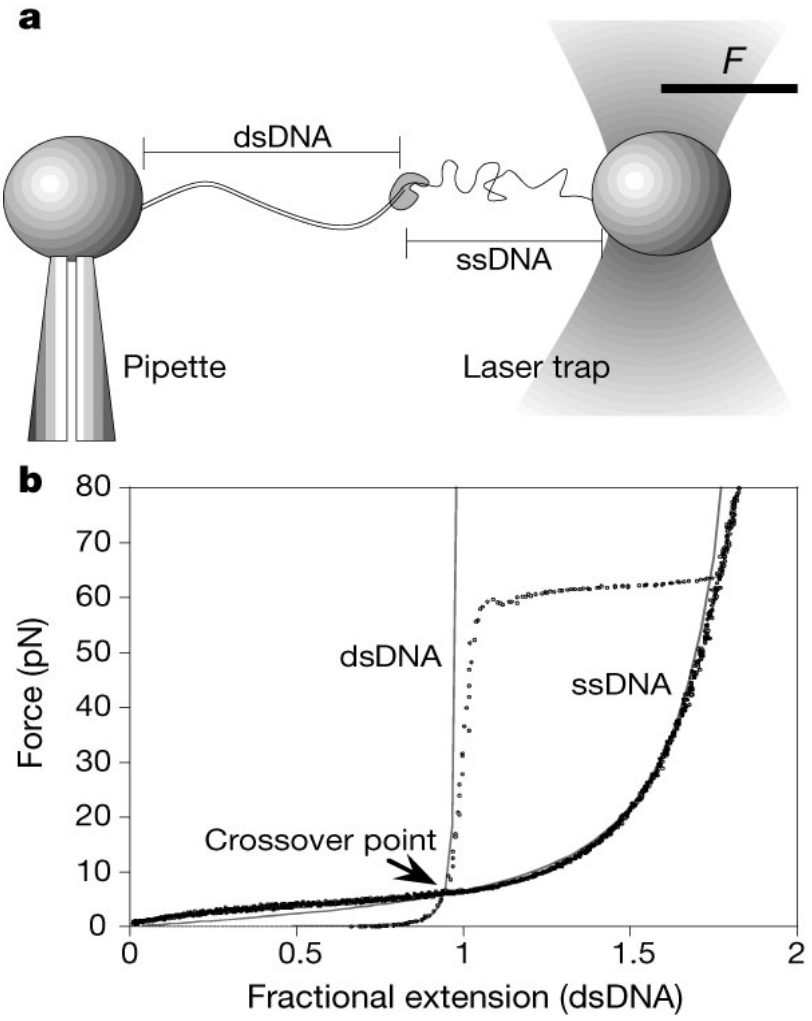

Fig. 25. Measurements of replication by single DNA polymerase molecules. (a) Single-stranded DNA is converted to double-stranded DNA, changing the elasticity of the tether. (b) Elasticity curves for dsDNA and ssDNA showing that under constant force the extension will change as DNA is converted to ds-form. Reprinted with permission from *Nature* **404**, 103 (2000).

Fig. 26

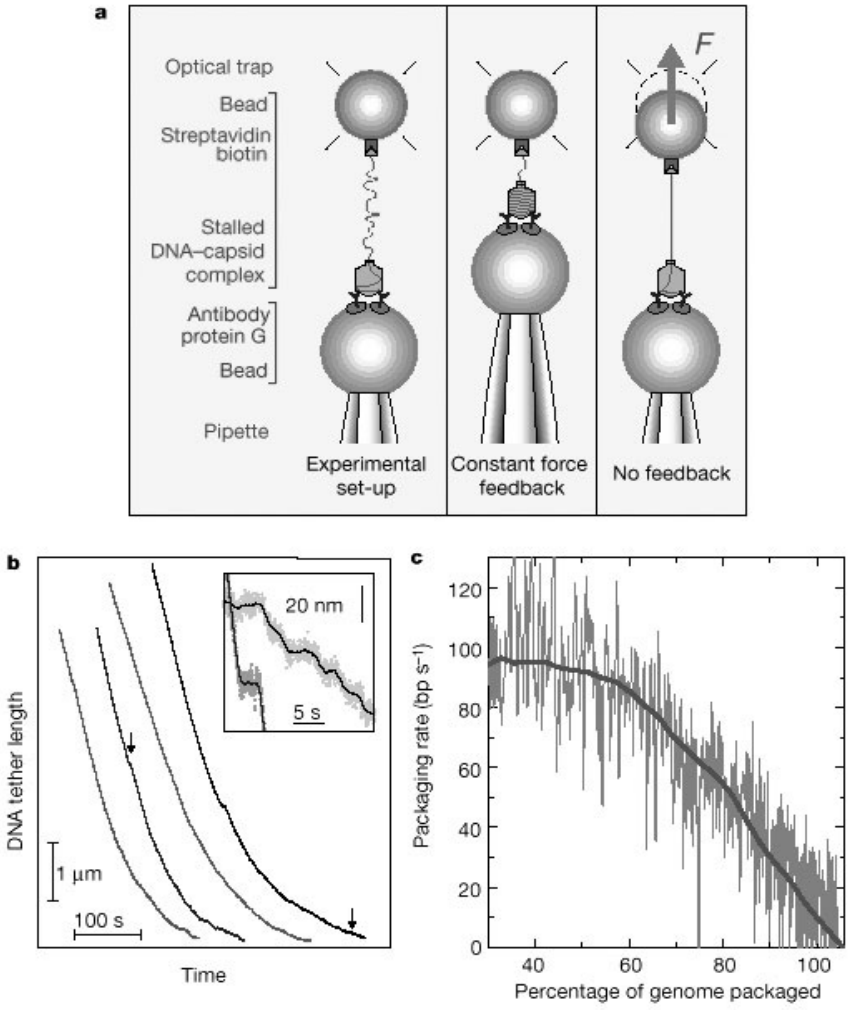

Fig. 26. Optical tweezers measurement of the packaging of a single DNA molecule by a single virus. (a) Schematic of setup showing feedback and no-feedback data recording modes. (b) Shortening of the DNA tether as it is packaged under a load of 5 pN in saturating ATP. (c) Reduction in packaging rate as the viral genome is packaged. Reproduced with permission from *Nature* **413**, 748 (2001).